Available online at www.sciencedirect.com
SCIENCE DIRECT®
Physica A 352 (2005) 53–112
PHYSICA A
www.elsevier.com/locate/physa

'Life is motion': multiscale motility of molecular motors ☆

Reinhard Lipowsky*, Stefan Klumpp

Max-Planck-Institute of Colloids and Interfaces, 14424 Potsdam, Germany

Available online 13 January 2005

Abstract

Life is intimately related to complex patterns of directed movement. It is quite remarkable that all of this movement is based on filaments and motor molecules which perform mechanical work on the nanometer scale. This article reviews recent theoretical work on the motility of molecular motors and motor particles that bind to cytoskeletal filaments and walk along these filaments in a directed fashion. It is emphasized that these systems exhibit several motility regimes which are well seperated in time. In their bound state, the motor particles move with a typical velocity of about 1 μm/s. The motor cycles underlying this bound motor movement can be understood in terms of *driven Brownian ratchets* and *networks*. On larger length and time scales, the motor particles unbind from the filaments and undergo peculiar *motor walks* consisting of many diffusional encounters with the filaments. If the mutual exclusion (or hardcore repulsion) of these motor particles is taken into account, one finds a variety of *cooperative phenomena* and *self-organized processes*: build-up of traffic jams; active structure formation leading to steady states with spatially nonuniform density and current patterns; and active phase transitions between different steady states far from equilibrium. A particularly simple active phase transition with spontaneous symmetry breaking is predicted to occur in systems with two species of motor particles which walk on the filaments in opposite directions.

PACS: 87.16.−b; 05.40.−a; 64.60.Cn

☆ http://www.mpikg.mpg.de/th/

*Corresponding author.
E-mail address: reinhard.lipowsky@mpikg-golm.mpg.de (R. Lipowsky).

0378-4371/$ - see front matter © 2005 Elsevier B.V. All rights reserved.
doi:10.1016/j.physa.2004.12.034

1. Introduction

More than 2000 years ago, Aristotle and his school noticed that everything in the natural world can be divided into two main categories, non-living objects and living organisms. They thought that these two categories can be distinguished by the different ways in which nonliving and living things move and that only living organisms can move 'on themselves', i.e., without external driving forces. This insight is summarized by the Aristotelian proverb 'Life is motion'.

Today, we know that living organisms have a complex internal architecture which is organized in a hierarchical fashion: all organisms are built up from cells and all cells contain complex assemblies of molecules. These structures cover a wide range of length scales. Roughly speaking, multicellular organisms have a linear size in the range from meters down to millimeters, cells from millimeters to micrometers, and molecular assemblies from micrometers to nanometers. All levels of this structural hierarchy are rather dynamic and *exhibit movements on many different time scales*.

On the scale of organisms, which we can observe with the naked eye, we encounter the intricate movements of animals and plants. Looking through a light microscope (or a good magnifying glass as used by van Leeuwenhoek), we can observe single cells which swim or crawl along surfaces. Finally, on the nanometer scale, we now have a variety of experimental methods, developed during the last decade, which reveal the direct movement of single motor molecules and the force generation of growing filaments. Furthermore, we now understand that *all* self-propelling and directed movements of living things ultimately arise from the cooperative action of such supramolecular assemblies.

There are several classes of molecular motors which fulfill different functions in the living cell [1]. Prominent examples are: (i) DNA and RNA polymerases, which move along the strands of DNA in order to replicate it and to transcribe it into RNA, respectively; (ii) membrane pumps which transport ions and small molecules across membranes; the resulting concentration gradients may be used in order to drive (iii) rotary motors such as the bacterial flagellar motor and the F_1-ATPase, which are used for cell locomotion and ATP synthesis, respectively; (iv) myosins in muscles which work in ensembles and collectively displace actin filaments; and (v) cytoskeletal motors which bind to the filaments of the cytoskeleton and then walk along these filaments in a directed fashion [2,3]. The latter class of motors is essential for intracellular transport, cell division, and cell locomotion.

Many of these motors are powered by the free energy released from the hydrolysis of adenosine triphosphate (ATP). From the molecular point of view, these motors have two remarkable properties. First, they represent ATPases, i.e., catalysts or enzymes for the hydrolysis of ATP. For the concentrations which prevail in living cells, the ATP hydrolysis is strongly exergonic but it is also quite slow in the absence of any enzymatic activity. The motors act as enzymes for this chemical reaction and strongly increase its reaction rate. Second, these molecular motors are also able to transform the free energy released from the ATP hydrolysis into mechanical work. In fact, this energy transduction occurs even on the level of *single* hydrolysis events. In this way, molecular motors consume the smallest possible amount of fuel.

One class of motors that are powered by ATP hydrolysis consists of cytoskeleton motors such as kinesin and myosin V, which move along cytoskeleton filaments such as microtubuli and F-actin. One example for such a pair of motor and filament is shown in Fig. 1. These cytoskeletal motors, which represent true nanomachines, are the main focus of this article. More precisely, the phenomena and processes discussed in this article apply to various types of 'motor particles' which may consist of (i) single molecular motors or (ii) cargo particles which are attached to a single molecular motor or (iii) cargo particles which are attached to several molecular motors.

From the conceptual point of view, the directed walks of cytoskeletal motors are quite remarkable since these motors are rather small. Each head of kinesin, e.g., has a linear size of the order of 10 nm, see Fig. 1 and will be easily perturbed by random thermal collisions with the adjacent water molecules. Therefore, the directed movement of these motor proteins directly reveals that they are able to escape from the surrounding 'molecular chaos'. In general, any nanoparticle in water will undergo erratic or Brownian motion which reflects the underlying thermal collisions and has *no* preferred spatial direction (in the absence of an external force field). However, one may imagine to *rectify* this random motion by a ratchet mechanism which corresponds to a rather simple and purely mechanical version of Maxwell's demon.

This article is organized as follows. First, Section 2 describes the basic properties of the different motility regimes. Next, Section 3 contains a brief review of Brownian motion and ratchets. In order to make many successive steps along the filament, each molecular motor must be able to undergo cycles of conformational states as discussed in Section 4. These motor cycles can be studied in the context of driven Brownian ratchets and networks and exhibit some universal properties. On time scales, which are large compared to their walking time, the molecular motors and motor particles undergo peculiar motor walks which are described for a variety of

Fig. 1. Two kinesin motors (without cargo) bound to a microtubule segment. The microtubule is built up from tubulin dimers and has a diameter of 24 nm. Each motor molecule has two motor domains or heads which are connected by a neck region and a long stalk. The total length of the kinesin molecule is about 80 nm. Each motor head can bind to the microtubule and, in the bound state, adsorb and hydrolyze ATP.

open compartments in Section 5. Interacting motor particles are discussed in Section 6 and are shown to lead to a variety of cooperative phenomena and self-organized processes: build-up of traffic jams; active formation of density and current patterns; phase transitions between different steady states. Finally, Section 7 gives a brief outlook on active biomimetic systems in general.

2. Motility regimes: basic properties

The movements of molecular motors and motor particles cover many length and time scales. As mentioned, the term 'motor particle' as used here stands for (i) a single molecular motor or (ii) a cargo particle which is attached to a single molecular motor or (iii) a cargo particle which is attached to several molecular motors. For a single motor particle, one can distinguish three different regimes: (i) the molecular dynamics of the motor proteins underlying the chemomechanical energy transduction which leads to a single step of the motor particle; (ii) the directed walks of this particle along the filaments; and (iii) the motor walks of the motor particle as it repeatedly unbinds from and rebinds to the filaments.

The molecular dynamics regime (i) covers all length scales up to the displacement of a single motor protein arising from the hydrolysis of ATP. Dimeric or two-headed kinesin walks by discrete steps which lead to center-of-mass displacements of 8 nm corresponding to the repeat distance of the microtubule [4]. Likewise, myosin V which also walks with two heads makes steps which lead to a center-of-mass displacement of 36 nm, close to the helical pitch of the actin filaments [5]. For kinesin, the corresponding stepping time has been measured to be faster than 70 μs [6]. The time scale for a whole motor cycle is substantially longer and depends on the ATP concentration. For high ATP concentration, the cycle time becomes essentially independent of this concentration and is observed to be of the order of 10 ms. As one decreases the ATP concentration, the cycle time starts to increase when it becomes dominated by the diffusion-limited transport of the ATP molecules to the ATP adsorption domains of the motor heads.

The second motility regime (ii) corresponds to the directed walks of the motor particle in its bound state. If this particle is pulled by a single motor protein, these directed walks involve, on average, about 100 steps for kinesin and about 50 steps for myosin V and, thus, cover a walking distance of about 1 μm. The corresponding walking times are of the order of seconds for sufficiently large ATP concentrations. The walking distance can be substantially increased if the cargo is pulled by several motor proteins. In all cases, the directed walk along the filament will eventually be terminated by the unbinding of the motor particle from the filament, which reflects the finite binding energy of the motor particle/filament complex.

For length and time scales which exceed the walking distance and the walking time, respectively, one enters the third motility regime (iii) corresponding to motor walks in which the motor particle repeatedly unbinds from and rebinds to the filaments. In a typical motility assay, the filament is surrounded by an aqueous solution which contains ions and ATP. It may also contain a finite concentration of

unbound motor particles but this concentration is typically so small that one can ignore the interactions between the unbound particles. In such a situation, the viscosity of the aqueous solution is close to the viscosity of water, and the unbound motor particle undergoes diffusive motion with a diffusion coefficient which is of the order of square micrometers per second. On the other hand, if the motor particle unbinds from a filament in vivo, it can interact with a variety of macromolecules, filaments, membranes, and organelles which tend to substantially reduce its diffusive motion. Thus, in vivo, the unbound motor particle will often stay close to its detachment point, and its directed movement will be interrupted by periods in which the motor appears to rest. This seems to happen in slow axonal transport of neurofilaments where rapid movement is interrupted by prolonged pauses [7,8].

So far, we have discussed a single motor particle which one may monitor by fluorescence labeling and single particle tracking. The different motility regimes just described should be accessible to such experimental studies as long as the motor particle concentration is sufficiently low and one may ignore their mutual interactions. It is important to keep in mind, however, that the motor particles considered here are processive in the sense that they make many steps when bound to the filaments. This is only possible if their binding energy is large compared to the thermal energy T (here and below, we will use the symbol T to denote the temperature in energy units). This implies that the equilibrium between the bound and the unbound state of the motor particle is strongly biased towards the bound state, and the filaments become already overcrowded with bound motor particles even if the overall number density of these particles is still relatively small. In such a situation, one must take the mutual exclusion or hard core repulsion between the bound motor particles into account.

The latter interactions are also present in the living cell. Consider, e.g., a neural cell and the transport along its axon as schematically shown in Fig. 2. Axons are tube-like structures enclosed by the plasma membrane of the neuron. The axon connects the cell body of the neuron with the axon terminal or synaptic cleft. The neurotransmitters which are released into the synaptic cleft are synthesized in the cell body and, thus, must be transported along the whole axon. This is quite remarkable since axons can be rather long.[1] Those axons, e.g., which connect our spine with our fingers and toes, are of the order of half a meter which is about 1000 times as long as the walking distance of the motor particles.

The cartoon in Fig. 2 indicates that the traffic within an axon can be rather dense and, thus, may lead to traffic jams. There is indeed some experimental evidence for jams of motor particles in axons (W. Saxton, private communication). An extreme case has been induced by mutations of the motor proteins which led to strong swelling of the axons [9,10]. Jams of kinesin-like motors have also been observed in fungal hyphae as one varied the motor concentration in vivo by changing the level of expression of the corresponding gene [11,12].

[1]The diameter of axons varies between hundreds of nanometers and millimeters. It would be interesting to know how the cross-sectional density of the filaments in different axons varies with their diameter.

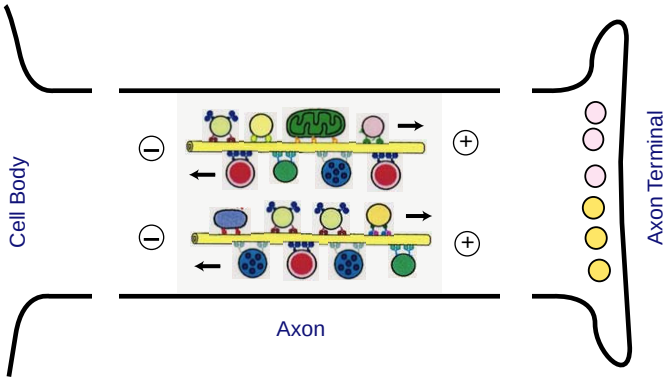

Fig. 2. Motor traffic in axons. Schematic view through an axon which contains many microtubules, oriented with their plus ends towards the axon terminal and with their minus ends towards the cell body. Cytoskeletal motors (indicated by small 'feet') are responsible for the transport of various types of cargo such as vesicles and organelles. Some species of motors walk towards the plus end of the filaments, others walk towards their minus ends. The traffic is rather crowded and can lead to traffic jams.

In the following, we will focus on motility assays or biomimetic systems in order to avoid the complexity of living cells. Thus, we will focus on relatively simple systems consisting of one or a few filaments which are immobilized within an open or closed compartment and which interact with populations of motor particles. We will see that these biomimetic systems exhibit a variety of cooperative phenomena and self-organized processes: build-up of traffic jams which have a strong effect on transport properties; active structure formation leading to steady states with spatially nonuniform density and current patterns; active phase transitions between different steady states far from equilibrium.

3. Of hot ratchets and cool demons

Molecular motors are rather small and have a size of 10–100 nm. Likewise, the cargo particles, which are moved by cytoskeletal motors, have a typical size of up to a few micrometers. This implies that all of these movements are necessarily overdamped, i.e., dominated by friction which transforms kinetic energy into heat. Three conceptual aspects of friction-dominated motion are discussed: Brownian motion, Brownian ratchets, and the relation between driven ratchets and Maxwell demons.

3.1. Brownian motion

Any nano- or microparticle in water will undergo Brownian motion which is erratic and nondirected. Such motion was first described by the botanist Brown who observed pollen particles in water through an optical microscope. As explained by Einstein and

Smoluchowski [13,14], Brownian motion arises from invisible collisions of the particle with adjacent water molecules and reflects the thermal motion of these molecules.

Now, assume that the particle is a cytoskeletal motor and that this particle is attracted towards a filament, compare Fig. 1. The bound particle may then undergo Brownian motion along the filament which corresponds to a random walk in one dimension. In the absence of fuel molecules, such random walks have been observed experimentally both for cytoskeletal motors bound to microtubuli [15] and for RNA polymerases bound to DNA [16].

The simplest description for Brownian motion in one dimension is provided by the Langevin equation. The position of the particle is described by the coordinate $x = x(t)$. The particle with mass m is subject to the friction force $F_{\rm fr} = -\phi(\mathrm{d}/\mathrm{d}t)x$, which is proportional to the velocity and to the friction coefficient ϕ. In addition, the particle is also driven by the random force $F_{\rm ra} = \zeta(t)$ which is Gaussian distributed with $\langle\zeta(t)\rangle = 0$ and $\langle\zeta(t)\zeta(t')\rangle = 2\phi T\delta(t-t')$ (as mentioned, temperature T is measured in energy units). The latter choice of the random force correlations is required in order to avoid inconsistencies with thermodynamics, see next subsections.

In the absence of additional external forces acting on the particle, one has the equation of motion

$$m\,\frac{\mathrm{d}^2}{\mathrm{d}t^2}\,x = F_{\rm fr} + F_{\rm ra} = -\phi\,\frac{\mathrm{d}}{\mathrm{d}t}\,x + \zeta(t)\,, \tag{3.1}$$

which can be easily solved by explicit integration. For large time t, one finds that the kinetic energy $\frac{1}{2}m\langle((\mathrm{d}/\mathrm{d}t)x)^2\rangle$ approaches the asymptotic value $\frac{1}{2}T$ as required by the equipartition theorem.

3.2. Brownian ratchets

One confusing aspect of Brownian motion is that the collisions with the water molecules both *damp* and *drive* the motion of the particle. Thus, mechanical movement is transformed into heat by friction and, at the same time, heat is transformed into mechanical movement. In the Langevin equation as given by (3.1), the damping is represented by the friction force and the thermal drive by the random force. For large time t, the dissipated power is given by $\langle((\mathrm{d}/\mathrm{d}t)x)\cdot F_{\rm fr}\rangle = -\phi\langle v^2\rangle = -\phi T/m$. This dissipated power is exactly cancelled by the work per unit time, $\langle((\mathrm{d}/\mathrm{d}t)x)\cdot F_{\rm ra}\rangle = \phi T/m$, which the random forces do on the particle.

At the beginning of the 20th century, this balance was only poorly understood and led to speculations that Brownian motion could be used in order to build a *perpetuum mobile* in the micrometer regime, see, e.g., Ref. [17]. It seems that this point was first clarified by Smoluchowski [18]. He considered the device shown in the left image of Fig. 3. A Brownian particle which consists of a ratchet with a sawtooth profile is constrained to move in one dimension. The sawtooth profile of the ratchet interacts with a pawl which consists of a spring and a wedge. One realization of such a ratchet is provided by a short segment of a cytoskeletal filament which is a polar and, thus, asymmetric rod-like object.

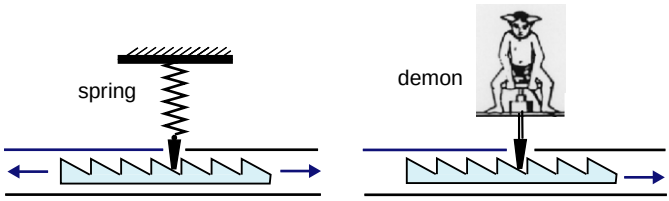

Fig. 3. (Left) Brownian ratchet with a sawtooth shape which could represent a filament segment. The ratchet is constrained to move only in one dimension, i.e., either to the right or to the left. The pawl consists of a spring which pushes a wedge against the sawtooth profile of the ratchet; and (Right) same device but with the spring replaced by a Maxwell demon.

The Brownian ratchet is subject to a random force arising from the thermal collisions with the surrounding liquid. This random force attempts to displace the ratchet to the right or to the left with equal probability. Inspection of Fig. 3(a) shows that the ratchet can move easily to the right, since the wedge can then slide over the sawtooth, but finds it difficult to move to the left since the wedge is then blocked by the sawtooth. Thus, the pawl seems to prevent displacements to the left, and one would naively conclude that the Brownian ratchet will, on average, move to the right. This would imply that the device is able to rectify random thermal fluctuations and could be used to transform heat directly into work. Such a device would correspond to a perpetuum mobile which violates the second law of thermodynamics.

The directed motion of the Brownian ratchet is, however, impossible as long as the pawl has the same temperature as the ratchet. Indeed, the spring also undergoes thermal fluctuations which occasionally lift the wedge over the barrier of the sawtooth. In fact, the Brownian ratchet displayed in left image of Fig. 3 is equivalent to Brownian motion in a sawtooth potential, $U_o(x)$, which depends on the one-dimensional coordinate x and is periodic but asymmetric in x. This leads to the additional force $F_o(x) = -(\partial/\partial x)U_o(x)$ in the Langevin equation as given by (3.1).

In the presence of this additional x-dependent force, the Langevin equation becomes difficult to study and it is then more convenient to describe the system in terms of the time-dependent probability distribution for the position x and velocity $(\mathrm{d}/\mathrm{d}t)x$ of the Brownian particle. In the strong friction limit, one may essentially ignore the inertial term $m(\mathrm{d}^2/\mathrm{d}t^2)x$ and it is then sufficient to study the time-dependent probability distribution $P(x,t)$ for the particle position x alone [19]. This probability distribution satisfies the conservation law

$$\frac{\partial}{\partial t}\,P(x,t) + \frac{\partial}{\partial x}\,J(x,t) = 0\,, \tag{3.2}$$

where the current J has the Smoluchowski or Fokker–Planck form

$$J(x,t) = -D\left[\frac{\partial}{\partial x}\,V_o(x) + \frac{\partial}{\partial x}\right]P(x,t) \tag{3.3}$$

with the reduced force potential

$$V_o(x) \equiv U_o(x)/T \tag{3.4}$$

and the diffusion coefficient $D \equiv T/\phi$.

The analysis of this equation shows that the sawtooth potential acts to modulate the position probability of the Brownian particle on small length scales, which are comparable to the period of the sawtooth potential, but does not change its motion on larger scales which is still purely diffusive without any preferred direction. Thus, if the whole system is in equilibrium, one cannot extract useful work from such a device in accordance with the second law of thermodynamics.

3.3. Driven Brownian ratchets

Now, let us imagine that the wedge is not coupled to a spring but that it is controlled by a small creature which resembles the demon introduced by Maxwell [20]. Such a demon could watch the Brownian ratchet and keep the wedge down if a sawtooth approaches from the right but lift the wedge up if a sawtooth approaches from the left. It is then obvious that the ratchet will move to the right.

We know, of course, that the demon envisaged by Maxwell cannot exist because any animal, which has eyes for perception, a brain for computation, and arms for force transduction must consist of a very large number of cells and, thus, requires a certain minimal size (it is interesting to note that the idea of a Maxwell demon has been recently reinvented in the form of nanorobots). It turns out, however, that such a complex creature is *not* required in order to rectify thermal fluctuations. Indeed, such rectification can be performed by a demon which is completely 'blind' and 'dumb', and may simply consist of a pawl as in Fig. 3(a), provided this pawl is *not* in equilibrium with the ratchet slat. From the physical point of view, the simplest way to do this is to cool the pawl compared to the slat [21]. Thus, if the ratchet is hot and the pawl is cool, the device shown in Fig. 3 will rectify the thermal fluctuations and the particle will move to the right.

However, temperature differences or gradients are not useful in the context of biological systems that are essentially isothermal. Simple organisms attain the temperature of their environment, whereas higher organisms such as mammals regulate their temperature and keep it fairly constant. Therefore, the protein 'demons', which are effective in biological systems, are not driven by temperature gradients but by *nonequilibrium chemical processes* [22]. In some cases, these processes arise from concentration gradients across membranes. In most cases, they are provided by exergonic chemical reactions such as ATP hydrolysis.

Thus, if we replace the demon and the wedge in Fig. 3 by a cytoskeletal motor and add ATP to the solution, the ratchet corresponding to a cytoskeletal filament will indeed move in a directed fashion. This process will continue until the ATP hydrolysis has produced a sufficient amount of ADP and P, and the forward and backward reactions balance each other. Therefore, the external field to which the motor/filament system is coupled does not arise from a spatial gradient but from an unbalance in the concentrations of ATP, ADP, and P. In addition, it is essential that

the rate of ATP hydrolysis is rather slow in the absence of any catalyst or enzyme since this reaction then involves a large energy barrier. The catalytic action which reduces this energy barrier is provided by the motor molecules themselves. Thus, the chemical free energy stored in the ATP molecules is released when these molecules are adsorbed by these molecular motors (or other types of molecular machines). In this way, the ATP molecules provide a spatially distributed source of energy, which is only tapped at those locations where it can be directly transformed into mechanical work (or other types of useful energy).

4. Molecular motor cycles

Molecular motors have the ability to undergo a cyclic sequence of conformations or states. In contrast to macroscopic engines, these motor cycles are stochastic in character and can be described by driven Brownian ratchets and networks. As a result, one obtains a general classification scheme for the chemomechanical coupling of these motors.

4.1. Possible motor cycles of two-headed motors

One basic property of a motor (or any other machine) is its ability to cycle through a certain sequence of states. Thus, the motor starts in a certain initial state, undergoes a sequence of transitions between different states until it finally comes back to its initial one. In order to be specific, let us consider the motor cycle of two-headed motor molecules such as kinesin or myosin V.

For these motor proteins, the motor cycle presumably consists of alternating forward steps by the two heads which corresponds to 'head-over-head' or 'hand-over-hand' motion. A possible sequence of molecular conformations corresponding to one forward step of the motor is displayed in Fig. 4.

Natural kinesin is a dimeric protein built up from two identical amino-acid chains and, thus, has two identical heads. However, since the linear size of these heads is of the order of 10 nm, we should be able to break this symmetry by a small chemical modification of one of the two heads without affecting the motor's movement. Therefore, the two heads can be distinguished, at least in principle, and a full motor cycle corresponds to *two* successive forward steps as shown in Fig. 4.

In this figure, the two heads of kinesin are drawn as two connected 'match sticks' which can bind to the discrete lattice sites on the filament. The half cycle starts in the top state in which both heads are bound, the leading one (on the right) releasing ADP whereas the trailing one (on the left) adsorbing ATP. Next, the trailing head unbinds from the filament and moves forward by two lattice sites, see bottom state in Fig. 4, and the old trailing head has become the new leading head. Half a motor cycle is completed by the release of phosphate and the rebinding of the leading head. Now, we have interchanged the two heads and another sequence as shown in Fig. 4 brings us back into the original conformation of the motor molecule. During each half

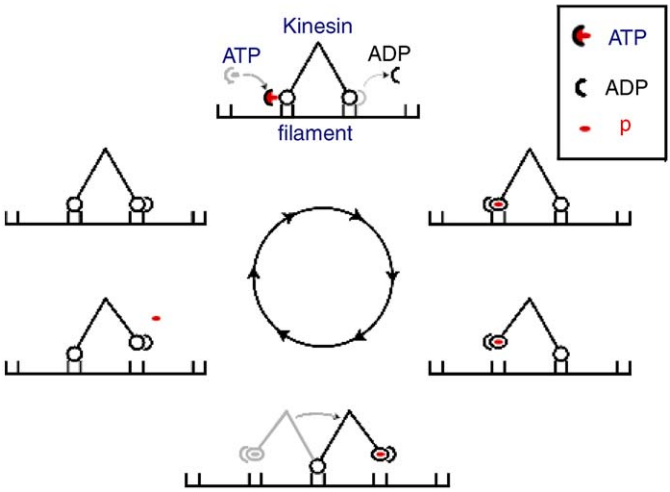

Fig. 4. Possible sequence of conformational states for 'hand-over-hand' motion. The six states shown here lead to a single forward step. After one such step, the leading and the trailing head have been interchanged. In order to attain its original conformation, the motor molecule has to make a second forward step and, thus, a second sweep through the conformational states shown here. Therefore, the full motor cycle corresponds to two such steps.

cycle, one head moves forward by 16 nm and the motor's center-of-mass moves forward by 8 nm.

There is now some direct experimental evidence that both two-headed myosin V on actin filaments [23] and two-headed kinesin on microtubules [24–26] step forward in such a 'hand-over-hand' manner. The precise sequence of conformations states corresponding to one forward step is not known, however, and the sequence shown in Fig. 4 represents only one possibility. In addition, one might also consider different kinds of forward steps such as 'inchworm' steps, see, e.g., Ref. [27]. It is important to realize, however, that *any* motor cycle must involve several stochastic processes because of the small size of the motor and because of its consumption of single fuel molecules.

4.2. Stochastic processes involved in motor cycles

Even in the absence of fuel molecules such as ATP, the molecular motor can attain many conformational states because of thermal collisions with the adjacent water molecules. Kinesin, e.g., is a rather large molecule, compare Fig. 1, and it will bend and rotate in various ways as a result of such collisions. In addition, when bound to a filament, a motor can undergo one-dimensional diffusion or 'passive sliding'. As mentioned, this has been observed both for dynein at microtubules [15] and for RNA polymerase at DNA [16].

The delivery of the fuel molecules represents another stochastic process since these molecules diffuse through the surrounding solution and will have several collisions with the motor molecule before they stick to the catalytic motor domains. For kinesin, this implies that the adsorption of ATP, which corresponds to the top state in Fig. 4, is a random process, and that the time for this adsorption step is governed by some probability distribution which depends on the ATP concentration. In fact, each step of the half cycle shown in Fig. 4 has such a stochastic character.

Finally, the motor can, in general, exhibit several possible pathways, which lead to a forward step, additional 'wrong' pathways, which lead to a backward step, and futile pathways, which lead to no step at all. Kinesin, e.g., could make forward steps using both different kinds of 'hand-over-hand' cycles and 'inchworm' cycles. Likewise, this motor could make a backward step if the *leading* head detaches from the filament after it has adsorbed and hydrolyzed an ATP molecule.

In order to describe these different stochastic processes, it is necessary to construct motor models with different internal states and to incorporate the basic property that the ATP hydrolysis is not in chemical equilibrium. In the following subsections, two somewhat different classes of models will be described which both have these basic features. These two classes of models provide examples for an even larger class of models which will be refered to as active networks.

4.3. Brownian ratchets driven by nonequilibrium processes

The first class of models is provided by Brownian ratchets driven by nonequilibrium processes. In these models, one starts from Brownian ratchets with several internal states. Thus, the motor molecule is viewed as a Brownian particle which can attain several internal states, labeled by m, and which experiences, in each of these internal states, a certain molecular force potential, U_m, arising from the cytoskeletal filament. This force potential depends on the spatial coordinate x parallel to the filament. Since this filament is polar, the molecular force potentials $U_m(x)$ will again be asymmetric and might resemble the sawtooth potential considered in (3.2)–(3.4). Furthermore, the periodicity of the filament implies that the force potentials are taken to be periodic in x.

The Brownian ratchets described so far will exhibit some diffusive motion but will not exhibit any directed movements. In order to perform some directed movement, these ratchets must be coupled to and driven by another nonequilibrium process such as unbalanced chemical reaction. This coupling leads to unbalanced transitions between internal states m and m' of the Brownian ratchets. These unbalanced transitions do not obey detailed balance and drive the ratchet out of equilibrium.

The stochastic dynamics of the driven Brownian ratchet is described by probability densities $P_m(x,t)$ to find the motor particle at position x and in internal state m with $m = 1,\ldots,M$. For a given position x, the densities P_m may change (i) because of lateral diffusion in state m which leads to lateral currents J_m depending on the molecular force potentials U_m or (ii) because of transitions between the different internal states. Therefore, the probability densities P_m satisfy the continuity equations

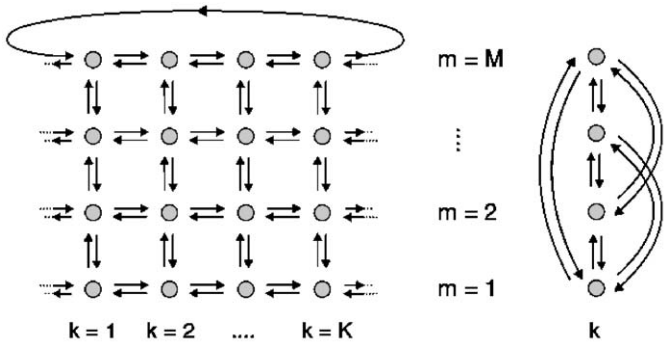

Fig. 5. Discrete Brownian ratchet with KM discrete motor states represented by vertices (k,m) with $1 \leqslant k \leqslant K$ and $1 \leqslant m \leqslant M$. The different values of k correspond to different spatial locations $x = x_k$ at which the Brownian ratchet can undergo transitions between the different internal states labeled by m. The latter transitions are indicated by the vertical arrows or directed edges. The horizontal arrows or directed edges represent diffusive transitions of the motor in state m. (Left) The network satisfies periodic boundary conditions in the longitudinal direction parallel to the k-axis; and (Right) it has an arbitrary number of transverse dimensions.

$$\partial P_m(x,t)/\partial t + \partial J_m(x,t)/\partial x = I_m(x,t) \quad \text{with } m = 1,\ldots,M\,, \tag{4.1}$$

with the transition current densities I_m. As explained in Appendix A, it is then convenient to consider transition current densities which are localized at K spatial locations $x = x_k$. In this way, one obtains a discretization of the Brownian ratchet which corresponds to a network of KM states as shown in Fig. 5. These (M,K)-models have been introduced and studied in Refs. [28–32] and represent generalizations of those considered in Refs. [33–35] with $(M,K) = (2,2)$. Somewhat different stochastic models for molecular motor cycles have been studied in Ref. [36]. An extended review about Brownian ratchets and related models is given in Ref. [37].

The discrete Brownian ratchets obtained in this way have one distinguished direction which corresponds to the x coordinate parallel to the filament. Since the molecular force potentials are periodic in x, the discrete Brownian ratchets satisfy periodic boundary conditions in this directions as indicated in the left part of Fig. 5. The transitions parallel to this x-direction are indicated by the horizontal arrows or directed edges in this figure. All of these horizontal transitions represent diffusive movements in the force potentials $U_m(x)$. In contrast, the vertical arrows or directed edges in Fig. 5 represent transitions between two different internal states, m and m'.

It is possible to analyze some properties of these discrete ratchet models for arbitrary values of K and M. For each value of k, one has a network 'slice' which consists of vertical transitions between different internal states m and m' as shown in the right part of Fig. 5. Within a certain 'slice', one can have up to $M(M-1)$ such transitions. Nearest neighbor 'slices' are connected by the horizontal transitions parallel to the x coordinate.

In the steady state, the motor is in state (k,m) with probability $P^{\rm st}(k,m)$. The transition rates from (k,m) to $(k+1,m)$ and vice versa are denoted by

$W(k,m|k+1,m)$ and $W(k+1,m|k,m)$, respectively. Using these rates, one can calculate the excess current $\Delta J^{\rm st}(k,m|k+1,m)$ from (k,m) to $(k+1,m)$ via

$$\Delta J^{\rm st}(k,m|k+1,m) = P^{\rm st}(k,m)W(k,m|k+1,m) - P^{\rm st}(k+1,m) \times W(k+1,m|k,m)\,. \tag{4.2}$$

The velocity $v_{\rm b}$ of the bound motor is proportional to the total steady-state current $J_{\rm tot}$ flowing through the discrete Brownian ratchet in the direction parallel to the filament. The latter current is given by

$$J_{\rm tot} = \sum_{m=1}^{M} \Delta J(k,m|k+1,m)\,, \tag{4.3}$$

which does not depend on the choice for the pair $(k,k+1)$.

One advantage of these ratchet models is that one can incorporate an externally applied force, F, in a rather direct and natural way. More precisely, one can incorporate the force component which is parallel to the filament and, thus, to the x coordinate. If we use the convention that positive values of F push the motor particle towards larger values of x, one has to study the Brownian ratchets with the generalized force potentials

$$V_m(x) \equiv [U_m(x) - Fx]/T\,, \tag{4.4}$$

which consist of both the molecular force potentials $U_m(x)$ and the externally applied force potential, Fx. This property does not apply, in general, to the second class of models described in the next subsection.

4.4. Cyclic networks for 'hand-over-hand' motion

In the second class of models, we consider the 'hand-over-hand' motion of two-headed motor molecules such as kinesin or myosin V. A possible sequence of conformations for the forward step of a single motor head is shown in Fig. 4. As mentioned, the full motor cycle consists of two successive steps performed by one head after another.

This motor cycle can be directly mapped onto the cyclic network shown in the left part of Fig. 6. In this figure, each edge represents two directed edges corresponding to two transitions into opposite directions. Thus, the motor makes forward steps if it follows the edges in the clockwise direction and backwards steps by following these edges in the counterclockwise direction. Likewise, the motor can make futile steps if it makes less than six successive transitions in the clockwise direction but then returns to its starting point before completing a half cycle.

The motor cycle shown in the left part of Fig. 6 is particularly simple since it consists of 12 states which form a single cycle. In general, the motor molecule may attain additional states as shown in the right part of Fig. 6. In this case, there are additional states which lead to other types of forward or backward steps as well as to additional types of futile steps.

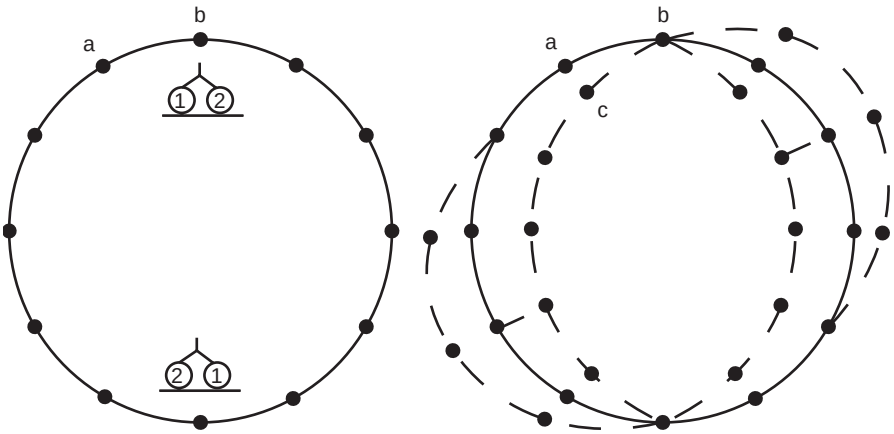

Fig. 6. Two networks corresponding to two possible motor cycles for 'hand-over-hand' motion. The vertices of the network correspond to the states of the motor, the edges which represent two directed edges in opposite directions correspond to the transitions between these states. (Left) Motor cycle consisting of a single cycle of states. Half of this cycle represents one step of one motor head as shown in Fig. 4. One forward step correspond to one half cycle with a clockwise orientation, one backward step to one half cycle with a counterclockwise orientation. Futile steps correspond to less than six clockwise transitions followed by the same number of counterclockwise ones; (Right) Motor cycle consisting of several pathways. The main pathway (full edges) is the same as on the left. In addition, there are additional states which lead to different types of backward and forward steps (interior broken edges), and different types of futile steps (exterior broken edges).

For the motor cycle networks displayed in Fig. 6, the velocity $v_{\rm b}$ of the motor molecule is again proportional to some excess currents in the steady state. For the motor cycle shown in the left part of Fig. 6, the velocity $v_{\rm b}$ is proportional to the excess current

$$\Delta J^{\rm st}_{ab} = P^{\rm st}_a \omega_{ab} - P^{\rm st}_b \omega_{ba} \tag{4.5}$$

from vertex a to vertex b where $P^{\rm st}_a$ and $P^{\rm st}_b$ are the steady-state probabilities to find the motor in state a and b, respectively, and ω_{ij} is the transition rate from vertex i to vertex j. Likewise, for the motor cycle in the right part of Fig. 6, this velocity is proportional to

$$\Delta J^{\rm st}_{ab} + \Delta J^{\rm st}_{cb} = P^{\rm st}_a \omega_{ab} - P^{\rm st}_b \omega_{ba} + P^{\rm st}_c \omega_{cb} - P^{\rm st}_b \omega_{bc} \, . \tag{4.6}$$

4.5. Driven Brownian networks

Both classes of models as described in the two previous subsections lead to networks of discrete motor states. In both cases, the motor states are represented by vertices and the transitions between these states correspond to (directed) edges between the corresponding vertices. Both classes of models provide examples for driven Brownian networks which are defined by the following rather general properties.

We consider an arbitrary graph with N_v vertices i which represent the different states of the system. The system can undergo transitions from state i to state j with transition rate ω_{ij} and from state j to state i with transition rate ω_{ji}. In the network graph, this pair of transitions is represented by a (nondirected) edge between the vertices i and j. The total number of edges within the network is denoted by N_e.

The probability $P_i(t)$ to find the system in state i now satisfies the master equation

$$\partial P_i(t)/\partial t = \sum_j{}' \left[P_j(t)\,\omega_{ji} - P_i(t)\,\omega_{ij}\right], \tag{4.7}$$

where the prime indicates that the summation is restricted to $j \neq i$. In the steady state, the time-independent probabilities $P_i = P_i^{st}$ satisfy the relationships

$$0 = \sum_j{}' (P_i^{st}\,\omega_{ij} - P_j^{st}\,\omega_{ji}). \tag{4.8}$$

This set of coupled but linear equations can be solved using a graph theoretic method as explained in Appendix B.

4.6. Transition rate dependence of steady-state currents

Using the general solution of the steady-state master equation (4.8), one may express all excess currents

$$\Delta J_{ij}^{st} = P_i^{st}\,\omega_{ij} - P_j^{st}\omega_{ji} \tag{4.9}$$

in terms of the transition rates ω_{ij}. These functional relationships have certain universal features. This was first shown for driven Brownian ratchets using a transfer matrix formalism [30–32]. These universal features will now be rederived and generalized to all driven Brownian networks.

The graph theoretic solution described in Appendix B implies that all excess currents can be written in the form

$$\Delta J_{ij}^{st} = \frac{\mathrm{Pol}_{ij}^{(1)}(\{\omega\})}{\mathrm{Pol}_{ij}^{(2)}(\{\omega\})} \tag{4.10}$$

with the two polynomials

$$\mathrm{Pol}_{ij}^{(1)}(\{\omega\}) \equiv \Omega_i\omega_{ij} - \Omega_j\omega_{ji} \tag{4.11}$$

and

$$\mathrm{Pol}_{ij}^{(2)}(\{\omega\}) = \Omega = \sum_i \Omega_i \tag{4.12}$$

as follows from (B.7) where the notation $(\{\omega\})$ indicates that both polynomials depend on many transition rates ω_{ab} corresponding to different edges $\langle ab\rangle$. As explained in Appendix B, each term Ω_i consists of $N_{\mathscr{T}}$ transition rate products where $N_{\mathscr{T}}$ is the number of different spanning trees for the network graph. Each of these transition rate products contains $N_v - 1$ factors ω_{ab} where each edge $\langle ab\rangle$ occurs only once.

Therefore, the two polynomials $\mathrm{Pol}_{ij}^{(1)}$ and $\mathrm{Pol}_{ij}^{(2)}$ are *multilinear* in all transition rates. The polynomial $\mathrm{Pol}_{ij}^{(1)}$ consists of transition rate products where each product contains N_v different transition rates. Likewise, the polynomial $\mathrm{Pol}_{ij}^{(2)}$ consists of $N_\mathscr{T} N_\mathrm{v}$ transition rate products where each product contains $N_\mathrm{v} - 1$ different transition rates.

The polynomial $\mathrm{Pol}_{ij}^{(1)}$ as given by (4.11) can be re-expressed as a sum over all cycles of the network graph. More precisely, one has to include all cycles $\mathscr{C}_{ij,k}$ which contain the edge $\langle ij\rangle$. In general, there are many such cycles which are distinguished by the index k. Each cycle defines two directed cycles $\mathscr{C}_{ij,k}^{+}$ and $\mathscr{C}_{ij,k}^{-}$ which have a clockwise and counterclockwise orientation, respectively. This leads to the unbalance

$$\Delta\Omega_{ij,k} = \Omega(\mathscr{C}_{ij,k}^{+}) - \Omega(\mathscr{C}_{ji,k}^{-}) = \prod_{\langle ab\rangle} \omega_{ab} - \prod_{\langle ba\rangle} \omega_{ba} \tag{4.13}$$

corresponding to cycle $\mathscr{C}_{ij,k}$ where the products include all directed edges of the corresponding directed cycles $\mathscr{C}_{ij,k}^{+}$ and $\mathscr{C}_{ij,k}^{-}$.

In general, the cycle $\mathscr{C}_{ij,k}$ does not provide a spanning subgraph for the network graph. One must now consider all spanning subgraphs $\mathscr{B}_{ij,k,l}$ which contain the cycle $\mathscr{C}_{ij,k}$ but do not contain any other cycle. Thus, if we delete the edge $\langle ij\rangle$ from such a subgraph, we recover a spanning tree of the network graph. The different subgraphs $\mathscr{B}_{ij,k,l}$ which have these properties are distinguished by the index l.

The polynomial $\mathrm{Pol}_{ij}^{(1)}$ can now be expressed in terms of the cycle unbalances as given by (4.13). This leads to

$$\mathrm{Pol}_{ij}^{(1)}(\{\omega\}) = \sum_{k} \left(\Delta\Omega_{ij,k} \sum_{l} \prod_{\langle a'b'\rangle} \omega_{a'b'} \right) \tag{4.14}$$

where the last product contains all directed edges $\langle a'b'\rangle$ which belong to the spanning subgraph $\mathscr{B}_{ij,k,l}$ but do not belong to the cycle $\mathscr{C}_{ij,k}$. All of these edges $\langle a'b'\rangle$ are oriented towards the cycle $\mathscr{C}_{ij,k}$.

4.7. Detailed balance and unbalanced transitions

If the Brownian network satisfies detailed balance, one has the local conditions

$$P_i^{\mathrm{st}} \omega_{ij} = P_j^{\mathrm{st}} \omega_{ji} \tag{4.15}$$

for all edges $\langle ij\rangle$. As shown in Appendix B.4, these local conditions are equivalent to the global conditions that all cycle unbalances vanish, i.e.,

$$\Delta\Omega_{ij,k} = 0 \quad \text{for all cycles } \mathscr{C}_{ij,k} \,. \tag{4.16}$$

In fact, these conditions are fulfilled for all cycles if they are fulfilled for a fundamental set of cycles, see (B.22). In this case, all excess currents are identically zero.

Now, consider a Brownian network which is coupled to another energy providing process. This latter process may arise from mechanical stresses induced, e.g., by specific interactions with other structures, from electromagnetic fields such as light

which induces photo-isomeric transitions, or from chemical reactions which are out of equilibrium. In the case of molecular motors, the energy input is usually provided by the adsorption and hydrolysis of ATP. Therefore, in this latter case, the strength of the coupling depends on the ATP concentration and *vanishes as this concentration goes to zero*. It is therefore convenient to decompose the transition rates ω_{ij} as [30]

$$\omega_{ij} = \omega_{ij}^{\mathrm{db}} + \Delta_{ij} \,, \tag{4.17}$$

where the first terms $\omega_{ij}^{\mathrm{db}}$ satisfy the local and global detailed balance relations as given by (4.15) and (4.16), and the second term Δ_{ij} vanish for zero coupling between the network and the energy providing process.

In general, the coupling between network and energy providing process is expected to be localized in the sense that it affects only a certain subset of states and transitions within the network. In the case of a molecular motor, both the adsorption and the hydrolysis will depend on the conformation of the motor molecule. Indeed, adsorption can only occur if the corresponding ATP adsorption site of the motor is not occupied. Likewise, the hydrolysis will depend on some specific interactions between motor and filament.

A particularly simple situation occurs if the coupling between the Brownian network and the energy providing process affects only a single transition rate, say

$$\omega_{IJ} \equiv \omega_1 = \omega_1^{\mathrm{db}} + \Delta_1 \,, \tag{4.18}$$

where Δ_1 vanishes as the coupling strength goes to zero. It then follows from the general solution as given by (B.11) that all cycles through $\langle IJ \rangle$ carry a nonzero excess current. Thus, all di-edges $\langle ij \rangle$ which belong to such a cycle have an excess current $\Delta J_{ij}^{\mathrm{st}} \neq 0$. Furthermore, all of these nonvanishing excess currents have the general form

$$\Delta J_{ij}^{\mathrm{st}} = \frac{1}{\Omega} \sum_k \left(\Delta\Omega_{ij,k} \sum_l \prod_{\langle a'b' \rangle} \omega_{a'b'} \right) \tag{4.19}$$

as follows from (4.10), (4.12) and (4.14). The multilinearity of the polynomial terms then implies that

$$\Delta J_{ij}^{\mathrm{st}} = \frac{a_1 \Delta_1}{b_0 + b_1 \Delta_1} \,, \tag{4.20}$$

where the coefficients a_1, b_0, and b_1 do not depend on Δ_1. Likewise, if one defines the excess current, ΔJ, by the summation over *any* subset of edges, one also has

$$\Delta J = \sum_{ij}{}' \Delta J_{ij}^{\mathrm{st}} = \frac{a_1' \Delta_1}{b_0 + b_1 \Delta_1} \,, \tag{4.21}$$

where the prime at the summation sign indicates the chosen subset and $a_1' \equiv \sum' a_1$. Note that these current–rate relationships resemble the Michaelis–Menten relation for enzyme kinetics.

It is straightforward to include more transition rates which are affected by the coupling to the energy providing process. If we have two such transition rates, ω_1

and ω_2, all excess currents in the network have the form

$$\Delta J = \sum_{ij}{}' \Delta J_{ij}^{\mathrm{st}} = \frac{a_1 \Delta_1 + a_2 \Delta_2 + a_{12} \Delta_1 \Delta_2}{b_0 + b_1 \Delta_1 + b_2 \Delta_2 + b_{12} \Delta_1 \Delta_2} \ . \tag{4.22}$$

This expression becomes even simpler if the two unbalanced transitions emanate from the same vertex. In this case, the coefficients a_{12} and b_{12} vanish and the crossproducts $\Delta_1 \Delta_2$ are absent.

In general, if the network contains $Q \geqslant 3$ transition rates ω_{ij}, which are coupled to the energy providing process, all excess currents can be expressed as ratios of two polynomials which are multilinear in the Q transition rates Δ_{ij}. Furthermore, there are no crossterms involving several Δ_{ij} if the corresponding unbalanced transitions emanate from the same vertex. These current–rate relationships were first derived for the discrete Brownian ratchets shown in Fig. 5 [30–32].

4.8. ATP concentration dependence of motor velocity

The velocity v_{b} of the bound motor is proportional to a certain excess current ΔJ in the steady state both for the driven Brownian ratchets and for the stochastic networks describing 'hand-over-hand' motion. In order to transform the general current–rate relationships for driven Brownian networks into a relation between the motor velocity and the ATP concentration Γ_{ATP}, one has to relate the Q unbalanced transitions with this concentration.

By definition, all unbalanced transitions must vanish in the absence of any ATP which implies

$$\Delta_{ij} \sim \Gamma_{\mathrm{ATP}} \quad \text{for small } \Gamma_{\mathrm{ATP}} \ . \tag{4.23}$$

Likewise, all cycle unbalances must also vanish in this limit, i.e.,

$$\Delta\Omega_{ij,k} \sim \Gamma_{\mathrm{ATP}} \quad \text{for small } \Gamma_{\mathrm{ATP}} \ . \tag{4.24}$$

This implies that the motor velocity v_{b}, which is proportional to a certain excess current, behaves as

$$v_{\mathrm{b}} \approx \frac{g_1 \Gamma_{\mathrm{ATP}}}{h_0 + h_1 \Gamma_{\mathrm{ATP}}} \tag{4.25}$$

if one keeps the terms up to first order in Γ_{ATP} both in the numerator and in the denominator. It is interesting to note that this asymptotic expression is again of the same form as the Michaelis–Menten relation for enzyme kinetics.

A more detailed model is obtained if one resolves the different processes which are involved in the adsorption and hydrolysis of ATP. The latter reaction scheme is summarized by

$$\mathrm{ATP} \rightleftharpoons \mathrm{ADP} + \mathrm{P_i} \ , \tag{4.26}$$

where $\mathrm{P_i}$ denotes the phosphate ion. This reaction requires an enzyme in order to proceed with reasonable rates. In the present context, this enzymatic activity is provided by the catalytic domain of a motor head.

The forward reaction at this catalytic domain consists of three transitions: (i) adsorption of one ATP molecule at the empty catalytic motor domain; (ii) the ATP molecule is hydrolyzed corresponding to the forward direction in (4.26); and (iii) ADP and P_i desorb from the catalytic motor domain. On the other hand, the backward reaction consists of (i) adsorption of ADP and P_i at the empty catalytic motor domain, (ii) ADP and P_i combine into ATP corresponding to the backward direction in (4.26); and (iii) ATP desorbs from the catalytic domain.

The transition rate for ATP adsorption depends on the ATP concentration $\Gamma_{\rm ATP}$. The simplest assumption for this dependence is given by

$$\Delta_{ij} = \kappa_{ij}\Gamma_{\rm ATP} \tag{4.27}$$

where state i has an empty catalytic domain. Likewise, the transition rate for ADP adsorption depends on the ADP concentration. In the limit of small ADP concentration, which corresponds to chemical nonequilibrium, one may simply ignore the latter transition.

If the motor has a single head, one expects to have only one adsorption transition in the motor cycle network which implies $Q = 1$. If the motor has two identical heads, one will have $Q = 2$ if *both* heads must be in a unique conformational state in order to have an ATP hydrolysis reaction at *one* of these heads. In general, one would expect that each head of a two-headed motor should have a unique state in order to become catalytic, but the second head may still have some conformational freedom. If one head can be active for two or three different conformations of the other head, one has $Q = 4$ or $Q = 6$, respectively. If the two heads are not identical as applies, e.g., to certain kinesin constructs, one could also imagine motor cycles characterized by $Q = 3$ or $Q = 5$. Larger values of Q are obtained if one considers the movement of several motor molecules which are bound to the same cargo.

If one assumes that the unbalanced transition rates are given by the simple linear relations (4.27), one obtains the general relationships [30]

$$v_{\rm b}(\Gamma) = \left[\sum_{n=1}^{Q} g_n \Gamma^n\right] \Big/ \left[\sum_{n=0}^{Q} h_n \Gamma^n\right] \quad \text{with } \Gamma \equiv \Gamma_{\rm ATP} \tag{4.28}$$

for the dependence of the motor velocity $v_{\rm b}$ on the ATP concentration $\Gamma \equiv \Gamma_{\rm ATP}$. Thus, the velocity $v_{\rm b}$ can be expressed in terms of the ratio of two Γ-polynomials of degree Q. The same relationships are obtained if one assumes that the unbalanced transition rates depend on Γ according to

$$\Delta_{ij} = \kappa_{ij}\Gamma/(1 + \Gamma/\Gamma^*_{ij})\,, \tag{4.29}$$

which represents a generalization of (4.27).

The velocity–concentration relationships as given by (4.28) were first obtained in the context of driven Brownian ratchets [30]. In the latter case, one may also include an externally applied force which enters the polynomial coefficients g_n and h_n and leads to a nonzero coefficient $g_0(F)$. In this way, one arrives at a classification scheme

for the functional dependence of the velocity on the *two* parameters Γ and F which agrees, for $Q = 1$, with the experimental observations on kinesin [38].[2]

5. Motor walks of noninteracting motor particles

In the previous section, we focussed on the movements of walking motors which are bound to filaments. Since the corresponding binding energy is necessarily finite, the motor can only make a certain number of steps before it unbinds from the filament. A single kinesin molecule, e.g., which has a step size ℓ of 8 nm, typically makes of the order of 100 steps before it unbinds. This implies the unbinding probability $\varepsilon_o \simeq 1/100$ per step. The corresponding walking distance $\Delta x_b \simeq \ell/\varepsilon$ is of the order of 800 nm. The same walking distance applies to a cargo particle which is pulled by a single motor molecules. A simple method to increase the walking distance for a certain type of cargo is to connect it to the filament with several motor molecules [39]. This is, in fact, the typical situation for vesicles or organelles which are transported within the living cell.

Thus, assume that n motors connect the cargo to the filament and that each motor has an unbinding probability ε_o per step. If the different motor molecules walked in an uncorrelated fashion, the unbinding probability for the cargo would be proportional to ε_o^n and the walking distance would scale as $\Delta x_{\rm b} \sim \ell/\varepsilon_o^n$. In general, one will expect, however, that motor molecules which pull the same cargo will interact in various ways; e.g., if one of these motors attempts to make a forward step, it may be hindered by another motor in front of it which then acts as a steric obstacle. On the other hand, if a motor completes such a forward step and pulls the cargo, it may also exert a pulling force on another motor behind it and, thus, may unbind this other motor. These two latter effects tend to reduce the walking distance $\Delta x_{\rm b}$. This distance represents a basic parameter of our models, and its value will be taken from experiments.

The models described in the following are applicable both to single motor molecules and to single cargo particles pulled by one or several motor proteins. As before, we will use the term 'motor particle' in order to describe both situations. On length scales which are small compared to the walking distance, the motor particles walk along the filament to which they are bound, and this directed movement is characterized by the bound state velocity, $v_{\rm b}$, which we have studied in the previous section, and the bound state diffusion coefficient, $D_{\rm b}$, which is discussed in Appendix C.2.

On length scales which are large compared to the walking distance $\Delta x_{\rm b}$, the motor particle undergoes peculiar 'motor walks' which arise from many diffusional encounters with the filament and, thus, consist of alternating sequences of bound and unbound motor states, i.e., of directed walks along the filaments and nondirected diffusion in the aqueous solution. When bound to a filament, the motor walks in a

[2]Strictly speaking, the force ramp used in Ref. [38] corresponds to a time-dependent external force which differs from the conservative force F included in (4.4).

certain direction until it unbinds; it then undergoes nondirected diffusive motion in the surrounding aqueous solution until it encounters the same or another filament to which it can rebind and continue its directed walk.

In this section, we discuss the motor walks performed by noninteracting motor particles. These walks are accessible in real systems provided the motor particle density is sufficiently small. As one increases this density, the mutual interactions of the motor particles become more and more important and affect their movements. In the next section, we will discuss the corresponding motor traffic.

5.1. Motor walks in different types of compartments

Now, consider a system with noninteracting motor particles which are labeled in such a way that we can track them. We now monitor the walk of one of these particles. It is intuitively clear that the relative contributions of directed and diffusive motion to such a motor walk will depend on the number and arrangement of the filaments and on the confinement of the overall motion by additional surfaces [40].

Within the cell which contains many filaments and membranes, the diffusive motion of the unbound motor particle is strongly restricted by the close proximity of these intracellular structures. Thus, as the motor particle unbinds from a filament in vivo, it will often stay close to its detachment point, and its directed movement will be interrupted by periods in which the motor appears to rest. This seems to happen in slow axonal transport of neurofilaments where rapid movement is interrupted by prolonged pauses [7,8].

For motility assays, on the other hand, one typically has filaments which are immobilized on the surfaces of open compartments as indicated in Fig. 7. In this case, the motor particle will diffuse in the surrounding medium and may then make large excursions away from the filament. However, for all geometries shown in Fig. 7, the motor particle will always return to the filament eventually. This is, in fact, a general property of these motor walks which holds even in the infinite volume limit provided the length of the filament grows with the linear dimensions of the system.[3]

5.2. Lattice models for motor walks

It is convenient to map the random walks of the motor particles onto lattice random walks [40]. On the one hand, the parameters of these lattice models can be chosen in such a way that the motor walk has the observed statistical properties of a single motor particle. On the other hand, these models can also be used to study the collective behavior of many motor particles which interact in various ways.

In the simplest version of the model, the filament consists of a one-dimensional line of binding sites. It is straightforward to extend this model to include several protofilaments corresponding to a microtubule but one then has to introduce

[3]In the infinite volume limit, the motor particle will eventually return to an infinitely long filament provided the spatial dimension $d \leqslant 3$.

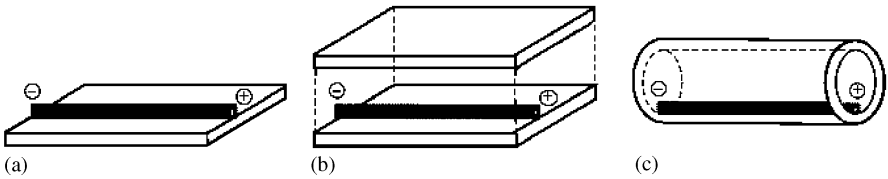

Fig. 7. Various compartments with one filament attached to the confining walls: (left) half space; (middle) slab; and (right) open tube. The filament corresponds to the thick rod with its minus end on the left and its plus end on the right. All three compartments are open in at least one spatial direction.

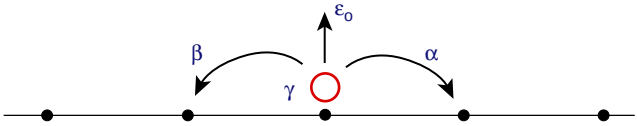

Fig. 8. Hopping probability for a motor particle located at a filament site. The particle moves forward (to the right) with probability α, backward (to the left) with probability β, unbinds from the filament with probability ε_o, and does not move with probability $\gamma = 1 - \alpha - \beta - \varepsilon_o$. For the simple cubic lattice considered here, the unbinding particle can reach one out of four nonfilament sites with probability $\varepsilon_o/4$. This model was introduced in Ref. [40].

additional parameters such as the probability to step from one protofilament to a neighboring one. Since these parameters are currently unknown, the following discussion is limited to the simplest filament model which consists of only one (proto)filament. In its bound state, the motor moves along the filament by making discrete steps of length, ℓ, which defines the lattice constant of the lattice model. For two-headed kinesin, the stepping length is 8 nm; for myosin V, it is 36 nm.

It is also convenient to discretize time and to assume that all moves of the motor particles occur at discrete time steps. Fig. 8 shows the different hopping probabilities for a motor particle which is located at a filament binding site. Within one time step, this motor particle stays at the same site with probability γ and unbinds from the filament with probability ε_o. Furthermore, this particle can make a forward step to the nearest neighbor filament site with probability α and a backward step to the other nearest neighbor filament site with probability β.

After the motor has unbound from the filament, it will undergo undirected diffusive motion on a three-dimensional lattice which is taken to be a simple cubic one. Thus, at each discrete time step, the motor particle can hop to one of its six nearest neighbor sites with equal probability. When the motor particle hops towards the filament, it binds or adsorbs to this filament with sticking probability π_{ad}.

The different hopping probabilities can be chosen in such a way that the motor particles have both the correct mean velocity, v_{b}, for the bound state and the correct diffusion coefficient, D_{ub}, for the unbound state. If one wants to match the bound diffusion coefficient, D_{b}, as well, one has to use two different time steps τ_{b} and τ, for the moves on the filament and away from it [40]. However, since the overall motor

walk is not very sensitive to the precise value of D_b, we also used a simplified parameter mapping in which the same time step is used for both types of moves [41,42]. These two parameter mappings are described in some detail in Appendix C.

5.3. Motor walks in two and three dimensions

The simplest systems in which one can study motor walks are provided by single filaments in unbounded geometries, i.e., without confining walls. In this case, one can use Fourier–Laplace transforms of the two- and three-dimensional lattice models in order to obtain analytical solutions for many quantities of interest [41,43]. These explicit solutions confirm and extend the results as obtained in Refs. [44] and [40] by scaling arguments.

Thus, let us consider an ensemble of noninteracting motor particles with a probability distribution which is initially localized at a single filament site. This initial distribution evolves with time into two distinct distributions, one for the bound motors, the other for the unbound motors. Both distributions are shifted in the forward direction parallel to the filament. For the bound motors, this leads to the average displacement shown in the left part of Fig. 9. In addition, the stochastic nature of the motor movements leads to a broadening of both the bound and the unbound motor distributions. This broadening can be characterized by the variance of the motor displacements as shown in the right part of Fig. 9 for the bound motors. Inspection of this figure also shows that the analytical results and the Monte Carlo data are in excellent agreement.

The effective diffusion coefficient D_b of the bound motors parallel to the filament is given by the slope of the variance displayed in the right part of Fig. 9. For large times, this diffusion coefficient attains anomalously large values in two dimensions and exhibits large logarithmic correction terms in three dimensions. Very similar

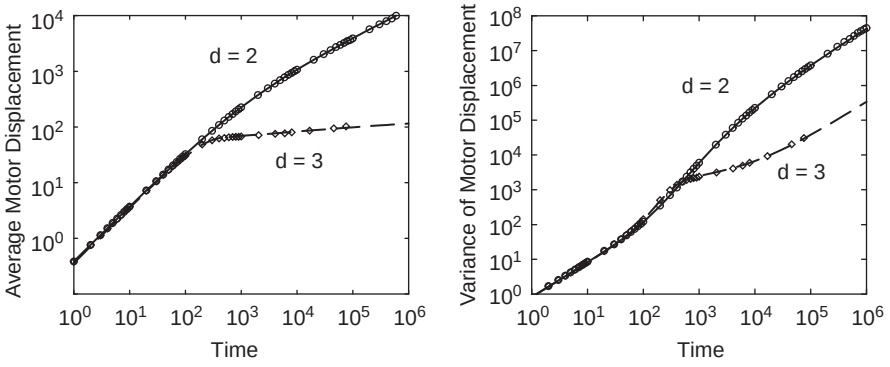

Fig. 9. Unbounded motor walks in two and three dimensions: (Left) Average displacement of bound motors parallel to the filament and (Right) Variance of displacements of bound motors as functions of time. The slope of this latter function defines the effective diffusion coefficient D_b which is anomalously large. In both plots, the curves represent analytical results for $d = 2$ and $d = 3$ dimensions whereas the circles and diamonds are the corresponding Monte Carlo data [41].

behavior is found for the diffusion of the unbound motors parallel to the filament. In addition, the diffusion is anisotropic since the perpendicular diffusion coefficients are smaller than the parallel ones. Therefore, the probability distributions for the unbound and bound motors are elongated parallel to the filament and are compressed perpendicular to it [41,43].

5.4. Motor walks in confined geometries

Next, consider systems in which the filament is immobilized on the surface or wall of a compartment as shown in Fig. 7. When the motor particles are placed into such a compartment, the motor walks will be affected by the compartment walls.

The systems shown in Fig. 7 consist of a single filament which is immobilized on the interior surface of a half space, slab, and tube. For all of these geometries, the motor still advances parallel to the filament but its average velocity decreases with time as shown in Fig. 10 [40]. In the half space, the motor velocity v decays $\sim 1/t$ for long times t and the advancement of the motor is so slow that it will be difficult to measure. In the slab, $v \sim 1/t^{1/2}$ and the advancement should be measurable if one tracks the motor for a couple of minutes. For an open tube which resembles an axon, the velocity is reduced by a constant factor which depends on the radius of the tube.

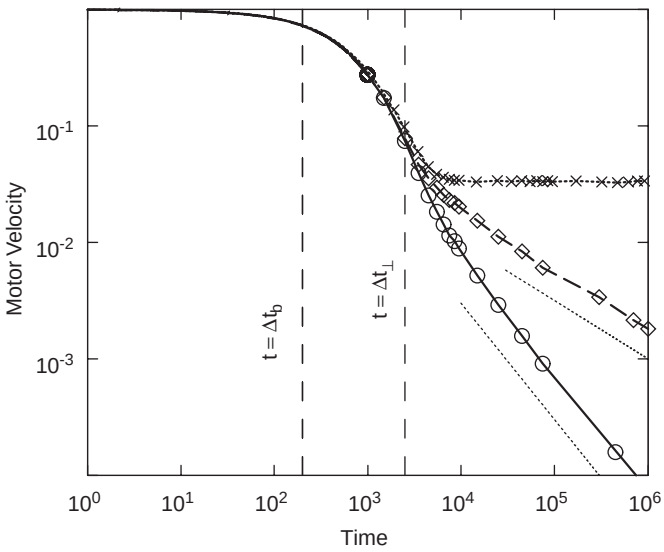

Fig. 10. The average motor velocity parallel to the filament as a function of time in the half space (circles), slab (diamonds), and tube geometry (crosses). Up to time $t = \Delta t_b$, the motors walk along the filament with the bound motor velocity v_b. The intermediate time regime up to $t = \Delta t_\perp$ is characterized by diffusive excursions which are small compared to the thickness of the slab or the diameter of the tube. Finally, for large t, the average velocity decays as $1/t$ and $1/t^{1/2}$ for the half space and the slab, respectively, but attains a constant value for the tube [40].

It is also of interest to study more complex arrangements of filaments. In particular, one may arrange these filaments in such a way that the motor particles undergo active diffusion with a diffusion coefficient which is much larger than the diffusion coefficient of normal Brownian motion [45].

6. Interacting motor particles

In the previous section, we have discussed the motor walks of noninteracting motor particles. Such walks will be observable if the motor particle density is sufficiently small and the system is sufficiently dilute. However, the motor particles considered here are characterized by a binding energy which is large compared to T. Otherwise, they could not make many steps along the filament. This implies that the equilibrium between the bound and the unbound state of the motor particle is strongly biased towards the bound state, and the filaments become already overcrowded with bound motor particles even if the overall number density of these particles is still relatively small. In such a situation, one must take the mutual exclusion or hard core repulsion between the particles into account [40,42].

6.1. Lattice models with mutual exclusion or hard core repulsion

It is straightforward to incorporate the mutual exclusion or hard core repulsion between the motor particles into the lattice models discussed in the previous section. In general, the size of these particles can vary and may exceed the lattice constant ℓ. Here, we will again focus on the simplest case for which this size is comparable to ℓ.

When bound to a lattice site of the filament, the motor particles have the same hopping probabilities as for the motor walks, but they can only complete their hopping attempts if the new lattice sites are not yet occupied. This is illustrated in Fig. 11 for a small cluster of three motor particles which represents a short traffic jam.

Our models are new variants of driven lattice gas models or exclusion processes, where the driving is localized to the filaments. Other variants of driven lattice gas models have been previously studied for a variety of transport processes, see, e.g., Refs. [46–52]; an extensive review of the one-dimensional asymmetric simple

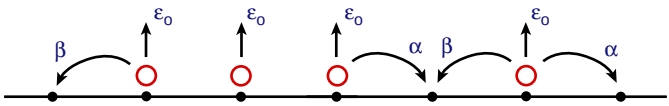

Fig. 11. Filament sites with three motor particles forming a small cluster (left) and one motor particle with no nearest neighbors (right). Each particle unbinds from the filament with probability ε_o; on the simple cubic lattice, it can then reach one out of four nonfilament sites with probability $\varepsilon_o/4$ provided the corresponding site is empty. Furthermore, each particle can make a forward step with probability α and a backward step with probability β if the new locations are not yet occupied. At each time step, each particle does not move with probability $\gamma = 1 - \alpha - \beta - \varepsilon_o$ [40,42].

exclusion process (ASEP) is contained in Ref. [53]. After our work on motor traffic along filaments had been published in Ref. [40], several groups have begun to study one-dimensional ASEPs in contact with particle reservoirs [54–56], which represent closely related systems.

6.2. Tube-like compartments

A rather simple system geometry is again provided by a single filament in a tube-like compartment which resembles an axon. Thus, consider such a geometry and increase the motor particle density by adding more and more of these particles to the system. This will also lead to an increase in the number of bound motors until this number saturates because the filament becomes overcrowded. This overcrowding has a rather strong effect on the transport along the filament. Indeed, if a motor wants to make a forward step, it can only do so if the next binding site at the filament is not yet occupied. Therefore, the overcrowding of the filament leads to traffic jams which strongly reduce the transport by the bound motor particles. These jams are similar to jams of locomotive engines on railroads; the main difference is that the engines considered here can unbind from and rebind to these railroads.

Even though the tube geometry with a single filament and a single motor species represents a rather simple transport system, it already exhibits a whole variety of different cooperative phenomena. These phenomena include: traffic jams leading to a nonmonotonic dependence of the bound motor current on the motor particle density; active formation of motor density and current patterns; and phase transitions induced by boundary densities.

In the following subsections, we will first define the basic tube geometry and then discuss the behavior of the motor particles for different boundary conditions at the tube ends. We start with open tubes with periodic boundary conditions which are useful in order to illustrate traffic jams and to obtain an intuitive understanding about the effect of traffic jams on the motor transport [42]. Simple examples for active pattern formation are found in tubular compartments with closed orifices [40]. Finally, tubular compartments, which are coupled to motor particle reservoirs at their orifices, lead to phase transitions between different steady states of the system [42].

6.2.1. Tube geometry and motor particle densities

We consider a cylindrical tube which contains a single filament, which may be located along the symmetry axis of the tube as shown in Fig. 12. The spatial coordinate parallel to the tube axis will be denoted by x. The tube has length L and radius R. Unless stated otherwise, the filament has the same length as the tube. Because of its polarity, the filament has two different ends, denoted by minus and plus. The motor particles considered in the following subsections move, on average, from the minus to the plus end. As before, these particles can unbind from the filament and then diffuse within the tubular compartment until they collide again with the filament and stick to it.

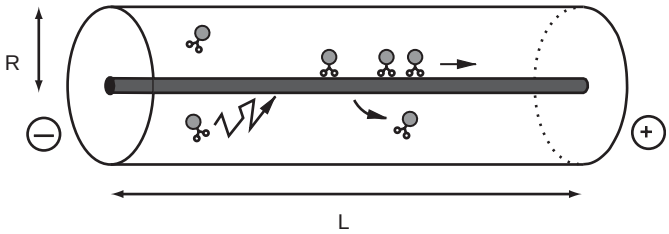

Fig. 12. Cylindrical tube of length L and radius R with a single filament located along the tube axis. When bound to the filament, the motor particles move, on average, from the minus to the plus end until they unbind from the filament. In the unbound state, these particle undergo nondirected diffusion within the tubular compartment until they rebind to the filament.

In the models discussed here, the motor particles move on a simple cubic lattice with lattice parameter ℓ. As for the motor walks, this length scale is taken to be the repeat distance of the filament. The tubular compartment is discretized in such a way that it consists of one line of binding sites, which represents the filament, and $N_{\rm ch}$ unbound 'channels', i.e., lines of lattice sites parallel to the filament. Thus the cross-sectional area A_o of the tube is equal to $A_o = (1 + N_{\rm ch})\ell^2$. For sufficiently large tube radius R, one has $A_o \approx \pi R^2$ which implies

$$\pi R^2 \approx (1 + N_{\rm ch})\ell^2 \,. \tag{6.1}$$

The number of motor particles within the tubular compartment is simply denoted by N. The corresponding motor particle number per tube length is defined by

$$\bar{N} \equiv N\ell/L \,. \tag{6.2}$$

Each motor particle can occupy one of the lattice sites which are labeled by i. Thus, if we look at a snapshot of the system, we will observe a certain configuration of motor particles which can be described by occupation numbers n_i with $n_i = 1$ if site i is occupied by a motor particle and $n_i = 0$ if it is not. In the following, we will focus on steady states of the systems which are characterized by time-independent density profiles

$$\rho_i = \langle n_i \rangle \quad \text{with } 0 \leqslant \rho_i \leqslant 1 \,. \tag{6.3}$$

These quantities represent local volume fractions. The particle number densities are then given by ρ_i/ℓ^3.

6.2.2. *Periodic boundary conditions*

In order to obtain a well-defined system, we have to supplement the tubular compartment with boundary conditions. From the theoretical point of view, it is most convenient to start with periodic boundary conditions as illustrated in Fig. 13. This system is translationally invariant parallel to the filament.

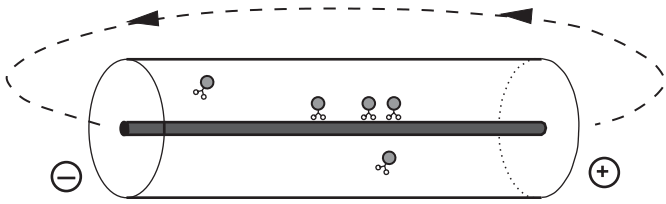

Fig. 13. Tubular compartment with periodic boundary conditions. Those motor particles which make a forward step at the plus end re-enter the system from the minus end. This system could be realized experimentally by a torus-like compartment.

In the steady state, the translational invariance has several consequences. First, the bound and unbound density profiles do not depend on the coordinate x parallel to the filament. Since there is no density variation of the unbound motors in the x-direction, there cannot be any current of the unbound motors parallel to the filament. It then follows that there cannot be any current of the unbound motors in the radial direction either. Therefore, the translational symmetry of the system leads to *detailed balance in the radial direction*. As a consequence, one can analytically calculate the densities and currents of the bound and unbound motors in the steady state [42].

Because of radial detailed balance, the x-independent densities $\rho_{\rm ub}$ and $\rho_{\rm b}$ of the unbound and bound motors satisfy the relation [42]

$$\rho_{\rm b} = \frac{\rho_{\rm ub}}{\varepsilon/\pi_{\rm ad} + (1-\varepsilon/\pi_{\rm ad})\rho_{\rm ub}} \quad \text{with } \varepsilon \equiv 3\varepsilon_o/2 \tag{6.4}$$

with unbinding probability ε_o and sticking probability $\pi_{\rm ad}$. These two parameters enter the properties of the steady state only in the form $\varepsilon/\pi_{\rm ad}$. Furthermore, the bound motors which have average velocity $v_{\rm b}$ generate the steady-state current $J_{\rm b}$ which is given by

$$J_{\rm b} = v_{\rm b}\,\rho_{\rm b}(1-\rho_{\rm b})\,, \tag{6.5}$$

while the unbound motors with constant density $\rho_{\rm ub}$ do not generate any current. The unbound density $\rho_{\rm ub}$ can be explicitly calculated by solving a quadratic equation, see [42], and is found to depend on (i) the motor particle number per tube length, $\bar{N}$, as defined in (6.2), (ii) the number $N_{\rm ch}$ of unbound channels parallel to the filament which is related to the tube radius via $N_{\rm ch} \approx \pi(R/\ell)^2$, and (iii) the probability ratio $\varepsilon/\pi_{\rm ad}$. The bound density and current are then obtained from (6.4) and (6.5), respectively.

The bound current $J_{\rm b}$ in the steady state is displayed in Fig. 14 where the analytical solution is compared with Monte Carlo data. This current increases linearly with the motor particle number $\bar{N}$ as

$$J_{\rm b}/v_{\rm b} \approx \frac{\bar{N}}{1+(\varepsilon/\pi_{\rm ad})N_{\rm ch}} \quad \text{for small } \bar{N}\,, \tag{6.6}$$

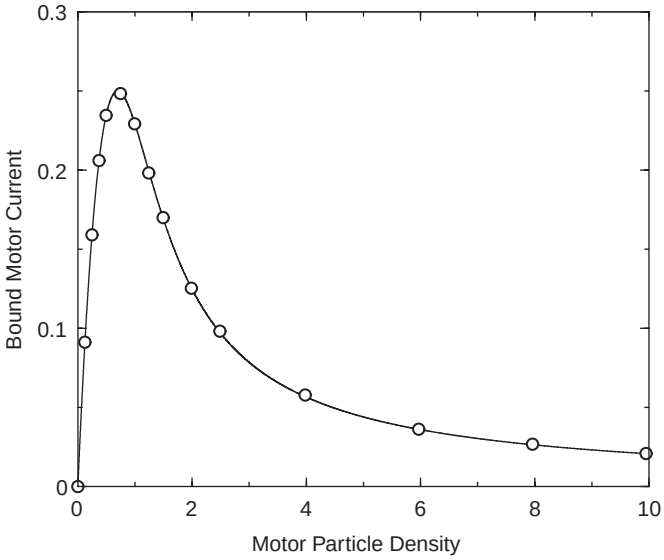

Fig. 14. Bound motor current J_b/v_b as a function of the motor particle density per tube length, $\bar{N}$. The tube has length $L/\ell = 200$ and radius $R/\ell = 25$ corresponding to channel number $N_{ch} = 1940$. The current attains its maximum at $\bar{N} \simeq 0.69$ and vanishes for $\bar{N} = 1 + N_{ch} = 1941$, i.e., when the tube is completely filled with motor particles. The curve represents the analytical solution, the open circles the Monte Carlo data [42].

attains its maximum value $\max(J_b/v_b) = 1/4$ for $\rho_b = 1/2$, $\rho_{ub} = (\varepsilon/\pi_{ad})/(1 + (\varepsilon/\pi_{ad}))$ and [42]

$$\bar{N} = \frac{1}{2} + \frac{\varepsilon/\pi_{ad}}{1 + \varepsilon/\pi_{ad}} N_{ch} , \tag{6.7}$$

and vanishes at $\bar{N} = 1 + N_{ch}$, i.e., when the tube is completely filled. The example shown in Fig. 14 corresponds to the parameter values $N_{ch} = 1940$ and $\varepsilon/\pi_{ad} = 10^{-4}$ which implies that the maximum is located at $\bar{N} \simeq 0.69$.

For small unbinding probability $\varepsilon_o = 2\varepsilon/3$, the ratio ε/π_{ad} becomes small, and the bound current J_b exhibits a rather narrow peak which is located at small motor particle numbers; this location attains its minimum value at $\bar{N} \approx 1/2$ in the limit of zero ε/π_{ad}. Thus, for small ε/π_{ad}, the motor transport is dominated by jams and the bound current J_b monotonically decreases for $1/2 < \bar{N} < 1 + N_{ch}$, i.e., for almost all accessible motor particle numbers. For small sticking probability π_{ad}, on the other hand, the ratio ε/π_{ad} becomes large, and the peak of the bound current is shifted towards large motor particle numbers. The location of the peak now attains its maximal value $\bar{N} \approx 1/2 + N_{ch}$ in the limit of zero π_{ad}, i.e., very close to complete filling of the tube. In this latter case, the current J_b increases monotonically with the number density $\bar{N}$ for $0 < \bar{N} < 1/2 + N_{ch}$.

The largest possible value for the unbinding probability is $\varepsilon_o = 1$ or $\varepsilon = 3/2$. In this limit, the peak is located at $\bar{N} = 1/2 + 3N_{ch}/5$, which is roughly in the middle of

the accessible range of motor particle densities. Thus, this peak is again rather broad provided the number of unbound channels, N_{ch}, is large.

6.2.3. Tubular compartment with closed orifices

The tube system considered in the previous subsection was translationally invariant parallel to filament and tube axis. The simplest way to break this translationally symmetry is by closing the orifices at the tube ends as indicated in Fig. 15. This leads to nonuniform densities both for the bound and for the unbound motors which now depend on the coordinate x parallel to the filament.

When bound to the filament, the motor particles walk again in a certain direction, say from the minus end to the plus end as in Fig. 15. However, when the bound particles reach the plus end, they can no longer step forward because of the closed orifice and thus will get stuck. The mutual exclusion or hard core repulsion of the bound motors now leads to the formation of a traffic jam which spreads from the plus towards the minus end. The jam is not completely static, however, since the bound motor particles can detach from the filament with small but finite unbinding probability ε_o. Therefore, once in a while, a motor particle will leave the jam by unbinding from the filament which creates space for some forward steps within the jammed region. In addition, the jam acts as a source of unbound motor particles, and the density of these unbound particles becomes nonuniform as well. Indeed, a density gradient of the unbound motor particles builds up with a higher density close to the plus end and a lower density close to the minus end. This density gradient leads to diffusive backflow of the unbound motor particles and to stationary states in which the bound current is balanced by this backflow current [40].

Some density profiles $\rho_b = \rho_b(x)$ for the bound motor particles are shown in Fig. 16(a). The three densities displayed in this figure correspond to three different motor particle numbers N. The tubular compartment has again length $L = 200\ell$ and radius $R = 25\ell$ or channel number $N_{ch} = 1940$ which leads to a total number of 200×1940 lattice sites. For $N = 40$, the bound density profile develops a rather short jam close to the plus end at $x = 200\ell$. This jam spreads towards the minus end with increasing

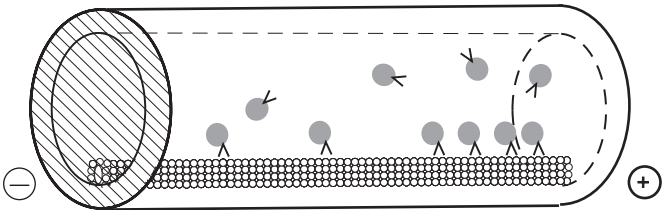

Fig. 15. Tubular compartment with closed orifices. The motor particles which arrive at the plus end get stuck until they unbind from the filament. Because of their mutual exclusion or hard core interaction, the bound motor particles form a jam which spreads from the plus end and builds up a density gradient for the unbound motor particles. The latter gradient induces a diffusive backflow of the unbound particles to the minus end [40].

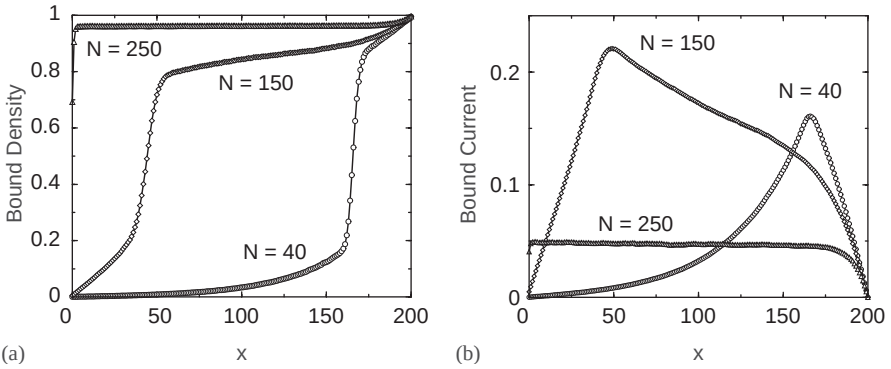

Fig. 16. (a) Bound density profiles $\rho_b = \rho_b(x)$ and (b) bound current profiles $J_b = J_b(x)$ as a function of the coordinate x (in units of ℓ) in a tubular compartment with closed orifices as shown in Fig. 15. The three different profiles correspond to three different values of the motor particle number N. The tube has length $L/\ell = 200$ and radius $R/\ell = 25$ corresponding to channel number $N_{ch} = 1940$ [40].

N and covers most of the filament for $N = 150$. As one reaches $N = 250$, the filament is completely covered and the density ρ_b is almost equal to its maximal value, $\rho_b = 1$.

Thus, for intermediate values of the motor particle number N, the filament in the closed tube consists of a crowded segment close to the plus end and a depleted segment close to the minus end. The corresponding density profiles $\rho_b(x)$ of the bound motor particles exhibit an interface between the crowded and the depleted region as in Fig. 16(a) for $N = 40$ and 150. The density profiles $\rho_{ub}(x)$ of the unbound motors have a similar shape but a much smaller magnitude. This steady state represents a simple example for active pattern formation, i.e. , for a nonuniform density pattern which is induced by active processes.

The density profiles lead to current profiles which vary with the filament coordinate x as well, see Fig. 16(b). The current profile $J_b = J_b(x)$ of the bound motors can be obtained from

$$J_b(x) = v_b\,\rho_b(x)(1-\rho_b(x)) - D_b\frac{\partial}{\partial x}\rho_b(x) \tag{6.8}$$

with the bound state diffusion coefficient D_b. In the cases discussed here, the contribution arising from the bound state diffusion is relatively small and one has $J_b(x) \simeq v_b\,\rho_b(x)(1-\rho_b(x))$ to a good approximation. Thus, the current profile $J_b(x)$ of the bound motors is small both in the depleted and in the jammed region but exhibits a maximum in the interfacial region where the density profile $\rho_b(x) = 1/2$ as shown in Fig. 16(b).

Since the motor particles cannot leave the closed tubular compartment, the current profile $J_b(x)$ of the bound motors must be exactly cancelled, in the steady state, by the current profile $J_{ub}(x)$ of the unbound motors. Therefore, one has the simple relation [40]

$$\int \mathrm{d}^2 z\, J_{ub}(x) = -J_b(x) \tag{6.9}$$

between these two current profiles where the integration extends over the whole cross-section of the tube. The overall transport along the filament can be characterized by the average bound current

$$\langle J_b \rangle \equiv \int dx\, J_b(x)/L\,, \tag{6.10}$$

which has again a maximum as a function of the motor particle density. In fact, the functional dependence of $\langle J_b \rangle$ on $\bar{N}$ is quite similar to the corresponding dependence of the uniform bound current J_b in the tubular compartment with periodic boundary conditions, see Fig. 13.

6.2.4. *Tubular compartments with motor particle reservoirs*

The two types of tubular compartments discussed in the previous subsections are characterized by a fixed number N of motor particles. Now, we will consider the situation in which the tubular compartments are coupled to two reservoirs of motor particles [42]. This coupling is again incorporated in the form of boundary conditions at the two orifices of the tube, see Fig. 17.

At the minus orifice, the tube is coupled to a motor particle reservoir which imposes the bound density $\rho_{b,in}$ at the minus end of the filament and the unbound density $\rho_{ub,in}$ at all other locations across this orifice. These two densities are taken to satisfy radial detailed balance in analogy to (6.4). This condition is convenient from a theoretical point of view but may not be easy to implement in an experimental system. In addition, at the plus orifice, the tube is coupled to another motor particle reservoir which imposes the bound density $\rho_{b,ex}$ at the plus end of the filament and the unbound density $\rho_{ub,ex}$ at all other locations across the orifice.

This system can exhibit three different phases—a low-density (LD) phase, a high-density (HD) phase, and a maximal current phase—in close analogy to the phases found in the asymmetric simple exclusion process in one spatial dimension. The corresponding phase diagrams are shown in Fig. 18. As shown in this figure, the precise form of the phase diagram depends on the relative length of filament and tube. If the filament has the same length as the tube (as in all previous cases), one obtains the phase diagram displayed in Fig. 18(a) which contains all three phases and is, in fact, identical with the phase diagram of the asymmetric simple exclusion process. On the other hand, if the filament length is somewhat shorter than the tube length, the filament gaps act as diffusive bottlenecks and the maximal current phase is lost for certain parameter values as shown in Fig. 18(b). Diffusive bottlenecks also

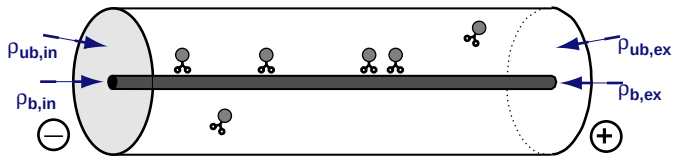

Fig. 17. Tubular compartment with its two orifices coupled to two motor particle reservoirs. For the orifice at the minus end, the bound motor density is $\rho_{b,in}$ and the unbound motor density is $\rho_{ub,in}$; for the orifice at the plus end, the bound and bound motor densities are $\rho_{b,ex}$ and $\rho_{ub,ex}$, respectively [42].

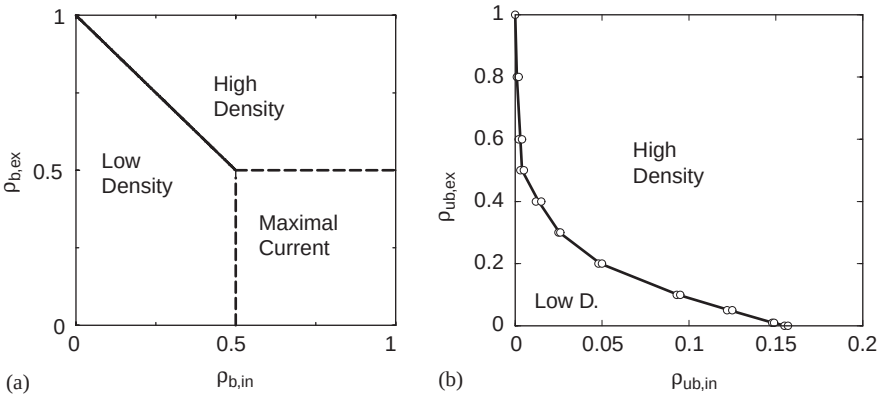

Fig. 18. Phase diagrams for two orifices coupled to two motor particle reservoirs. Case (a) corresponds to the situation in which filament and tube have the same length with boundary conditions as in Fig. 17. The phase diagram depends on the bound motor densities $\rho_{b,in}$ and $\rho_{b,ex}$ at the minus and plus end of the filament. Case (b) corresponds to the situation in which the filament is somewhat shorter than the tubular compartment. In this case, the phase diagram depends on the unbound motor densities $\rho_{ub,in}$ and $\rho_{ub,ex}$ at the minus and plus orifice [42].

affect the transport behavior of one-dimensional asymmetric simple exclusion processes as shown in Ref. [57].

Within the LD phase, the density profile $\rho_b(x)$ of the bound motors is essentially independent of x and satisfies $\rho_b(x) \simeq \rho_b^{LD}$ with $\rho_b^{LD} < 1/2$. Within the HD, the bound density profile $\rho_b(x)$ is given by $\rho_b(x) \simeq \rho_b^{HD}$ with $\rho_b^{HD} > 1/2$. Finally, the maximal current phase is characterized by $\rho_b(x) \simeq 1/2$ and a power-law decay of the density density correlation functions.

The phase transitions between the LD and HD phases are discontinuous while the transitions towards the maximal current phase are continuous. Therefore, a tubular compartment coupled to motor particle reservoirs exhibits a variety of non-equilibrium or active phase transitions. Even though the phase diagram depends on the precise form in which these reservoirs are coupled to the tube, it should be possible to realize such systems experimentally. One interesting example is provided by essentially closed compartments which are pierced by a filament: for such a system, the motor particles could only leave or enter when they are bound to the filament.

6.3. *Two species of motor particles*

So far, we have considered a single species of motors which walk on the filaments in a certain direction. In the cell, one has several species of motors which walk in opposite directions. For microtubules, kinesin motors walk typically from the minus to the plus end, whereas ncd motors walk from the plus to the minus end [3]. Likewise, myosin V and myosin VI motors walk towards the plus (barbed) and

minus (pointed) end of actin filaments.[4] The different motor species seem to compete for the same binding sites on the filaments [60].

In order to mimic this situation, we now consider two species of motor particles, 'plus' and 'minus', which move into opposite directions. As indicated by the notation, the plus motor particles move towards the plus end of the filament whereas the minus motor particles move towards its minus end. As in the case of a single motor species, we focus on the simplest compartment geometry which is again a tube with a single filament and periodic boundary conditions, compare Fig. 13. The following subsection is based on the results obtained in Ref. [61] where these model systems were introduced and shown to lead to active phase transitions.

6.3.1. Composition variables

In general, the two species of motor particles can have a different size and can occupy a different amount of space. For simplicity, we will take all motor particles to have the same volume equal to ℓ^3 where ℓ is the lattice parameter of our lattice models as before. This implies that the mole fractions of these motor particles are equal to the corresponding volume fractions.

For a tubular compartment of length L and radius R which contains N_+ plus motor particles and N_- minus motor particles, the volume fractions of the plus and minus motors are given by

$$\rho_+ \equiv \frac{N_+}{\pi R^2 L} \quad \text{and} \quad \rho_- \equiv \frac{N_-}{\pi R^2 L} \,, \tag{6.11}$$

respectively, which implies the total motor volume fraction

$$\rho \equiv \rho_+ + \rho_- = \frac{N_+ + N_-}{\pi R^2 L} \tag{6.12}$$

of all motor particles. The *relative* mole fraction Ψ of the minus motor particles is then given by

$$\Psi \equiv \frac{N_-}{N_+ + N_-} = \frac{\rho_-}{\rho} \quad \text{with } 0 \leqslant \Psi \leqslant 1 \,. \tag{6.13}$$

The system contains a majority of plus motors for $0 \leqslant \Psi < 1/2$ and a majority of minus motors for $1/2 < \Psi \leqslant 1$.

The relative mole fraction Ψ represents a useful control parameter for the system considered here. On the one hand, Ψ can be directly decreased or increased for an motility assay by adding more plus or minus motors to the aqueous solution, respectively. On the other hand, Ψ is genetically controlled in the living cell which regulates the gene activity for the corresponding motor molecules.

In general, the steady state of the system can be characterized by four populations of motor particles: bound plus, unbound plus, bound minus, and unbound minus; the corresponding numbers of motor particles are denoted by $N_{\mathrm{b},+}$, $N_{\mathrm{ub},+}$, $N_{\mathrm{b},-}$ and $N_{\mathrm{ub},-}$, respectively. The relative mole fraction Ψ_{ub} of the unbound motors is then

[4]The directionality of these molecular motors is sensitive to small changes in their molecular architecture and can be reversed by genetic engineering, see, e.g., Ref. [58,59].

given by

$$\Psi_{\rm ub} \equiv \frac{N_{\rm ub,-}}{N_{\rm ub,+} + N_{\rm ub,-}} \ . \tag{6.14}$$

This quantity is useful in the limit of large tube radius R for which the number of unbound motor particles becomes asymptotically equal to the number of all motor particles. Thus, one has

$$\Psi_{\rm ub} \approx \Psi \quad \text{for large } R \, . \tag{6.15}$$

For periodic boundary conditions as considered here, the steady state is translationally invariant parallel to the axis of the tube as for the case of a single species of motor particles, see Section 6.2.2. The system can then be characterized by four densities which are independent of the spatial coordinates: the bound and unbound densities $\rho_{\rm b,+}$ and $\rho_{\rm ub,+}$ of the plus motor particles as well as the bound and unbound densities $\rho_{\rm b,-}$ and $\rho_{\rm ub,-}$ of the minus motor particles. In this case, the relative mole fraction of the unbound motor particles is also equal to

$$\Psi_{\rm ub} = \frac{\rho_{\rm ub,-}}{\rho_{\rm ub,+} + \rho_{\rm ub,-}} \ . \tag{6.16}$$

6.3.2. Motor–filament and motor–motor interactions

In general, the two different species of motor particles may experience different motor–filament interactions which would lead to different hopping probabilities for single motor particles, compare Fig. 8. Indeed, the two types of motor particles may have different bound state velocities, different walking distances, and different sticking probabilities. However, all of these differences are expected to lead to smooth variations of the transport properties of the system. In order to reduce the number of model parameters, we will take all hopping probabilities for the plus and minus motor particles to be identical apart from the fact that they move in opposite directions. In particular, the bound state velocity of a single minus motor particle has the same magnitude as the bound state velocity of a single plus motor particle, i.e.,

$$v_{\rm b,-} = -v_{\rm b,+} \equiv -v_{\rm b} \ . \tag{6.17}$$

Likewise, both species of motor particles will be characterized by the same unbinding probability

$$\varepsilon_{o,-} = \varepsilon_{o,+} \equiv \varepsilon_o \tag{6.18}$$

and by the same sticking probability

$$\pi_{\rm ad,-} = \pi_{\rm ad,+} \equiv \pi_{\rm ad} \ . \tag{6.19}$$

The two species of motor particles may also experience different types of motor–motor interactions. First of all, all motors will again experience mutual exclusion or hard core repulsion. In typical cases, the overall volume fraction ρ is small, and the mutual exclusion is only effective for motors bound to the filament. In addition, the motor particles could be subject to attractive pair interactions. If these pair interactions were effective for the unbound motor particles, these particles would have a tendency to form clusters or domains in the solution. We do not know

of any experimental indications of such a behavior (even though it would be quite interesting from a theoretical point of view to study how clustering or phase separation of motor particles affects their transport along filaments). On the other hand, there is some evidence for attractive pair interactions between kinesin molecules bound to microtubules as will be discussed further below.

In the following, we will first consider the situation in which all motor particles experience mutual exclusion or hard core repulsion but no additional pair interactions. This leads to a smooth dependence of the steady-state currents on the relative mole fractions. On the other hand, the system with two species of motor particles undergoes a phase transition between two different steady states if two bound motor particles of the same species effectively attract each other.

6.3.3. Motor particles without attractive interactions

First, let us consider the situation in which the plus and minus motors exclude one another but do not experience any other type of interaction. In the limiting cases with mole fraction $\Psi = 0$, the system contains only plus motors and is thus equivalent to the systems discussed in subsection 6.2.2. For $0 < \Psi < 1/2$, one has a majority of plus motors within the tubular compartment. For the parameters chosen here, this also implies a majority of plus motors bound to the filament. With further increase of the relative volume fraction Ψ, the system is characterized by a majority of minus motors until one reaches the limiting case $\Psi = 1$. The latter case is again equivalent to the situation discussed in subsection 6.2.2.

As previously mentioned, the bound densities $\rho_{b,+}$ and $\rho_{b,-}$ and the unbound densities $\rho_{ub,+}$ and $\rho_{ub,-}$ are independent of the spatial coordinates because of the periodic boundary conditions. As in the case of a single species of motor particles, one has radial detailed balance which leads to

$$\varepsilon\rho_{b,\pm}(1-\rho_{ub}) = \pi_{ad}\rho_{ub,\pm}(1-\rho_b) \tag{6.20}$$

with $\varepsilon = 3\varepsilon_o/2$ and the densities

$$\rho_b \equiv \rho_{b,+} + \rho_{b,-} \quad \text{and} \quad \rho_{ub} \equiv \rho_{ub,+} + \rho_{ub,-} \,. \tag{6.21}$$

The quotient of the two relations contained in (6.20) leads to

$$\frac{\rho_{b,+}}{\rho_{ub,+}} = \frac{\rho_{b,-}}{\rho_{ub,-}} \,, \tag{6.22}$$

whereas the sum of these two relations implies that

$$\varepsilon\rho_b(1-\rho_{ub}) = \pi_{ad}\rho_{ub}(1-\rho_b) \,. \tag{6.23}$$

The latter relation is equivalent to (6.4) which expresses radial detailed balance for the system with a single species of motor particles.

As in the single species case, the steady-state current is again generated by the bound motors alone since there are no density gradients of the unbound motors. The total bound current, J_b, has now two contributions arising from the plus and minus motors. Mean field theory gives the explicit expression

$$J_b = J_{b,+} + J_{b,-} = v_b(\rho_{b,+} - \rho_{b,-})(1-\rho_b) \,, \tag{6.24}$$

where the relation $v_{b,-} = -v_{b,+} = -v_b$ has been used. Therefore, within mean field theory, the current J_b is proportional to

$$m_b \equiv \rho_{b,+} - \rho_{b,-} , \tag{6.25}$$

which plays the role of an *order parameter* for the system [61].

If one now varies the relative mole fractions Ψ, one finds a smooth variation of the bound densities $\rho_{b,+}$ and $\rho_{b,-}$ and, therefore, of m_b and J_b. For $0 \leqslant \Psi < 1/2$, the system contains a majority of plus motor particles which implies positive order parameter $m_b > 0$ and positive current $J_b > 0$. For $1/2 < \Psi \leqslant 1$, the system contains a majority of minus motor particles which implies negative order parameter $m_b < 0$ and negative current $J_b < 0$. As the relative mole fraction is varied from $\Psi < 1/2$ to $\Psi > 1/2$, both m_b and J_b change sign in a smooth fashion [61].

Therefore, if the different motor particles experience only hard core interactions, the system does not exhibit any phase transition. Such transitions arise, however, in the presence of additional, effectively attractive interactions between the bound motors as explained in the next subsections.

6.3.4. *Attractive interactions mediated by the filament*

Some information about the interactions between bound molecular motors has been obtained from decoration experiments using inactive (or nonmoving) motors. First, these experiments clearly demonstrate mutual exclusion from binding sites of the filaments. Second, there is evidence for an effectively attractive motor–motor interaction mediated via the filament. Such an interaction is implied by the coexistence of decorated and bare filaments, which has been observed both for the decoration of actin filaments by myosin [62,63] and for the decoration of microtubules by kinesin [64]. In the case of actin decoration, the motor–motor interaction depends on the internal conformation of the actin filaments [63]. This observation as well as experimental results on active kinesin in the presence of ATP [65] suggest that a bound motor leads to a localized deformation of the filament which promotes the binding of further motors on adjacent binding sites.

In order to incorporate these effectively attractive motor–motor interactions, a bound motor is now taken to increase the sticking probability π_{ad} for another motor of the same species to adsorb onto the adjacent filament site behind the bound motor (the term 'behind' is used here with respect to the direction in which this motor species walks). Likewise, the unbinding probability is taken to be reduced if another motor of the same species is located on the nearest neighbor filament site in the forward direction [61].

Let us assume that the binding rate π_{ad} is increased by a factor q and that the unbinding rate ε_o is decreased by a factor $1/q$ if another motor of the same species already occupies the forward neighbor site on the filament, see Fig. 19. These binding and unbinding processes obey detailed balance [42]. For steps along the filament, on the other hand, detailed balance is broken, and the corresponding rate α will, in general, change to α/q' with $q' \neq q$. We find that the system undergoes a phase transition for fixed q' and sufficiently large values of q. In order to eliminate one parameter, we will focus in the following on the situation with $q' = 1$. For an

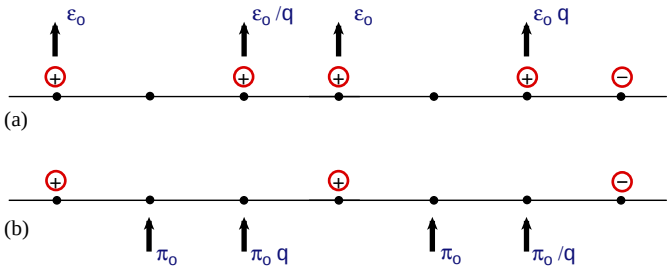

Fig. 19. (a) Unbinding probabilities for plus motor particles which are bound to the filament and move, on average, to the right as in Figs. 8 and 11. If the particle has no nearest neighbor in the forward direction, it unbinds with probability ε_o. If it is behind another plus motor, it unbinds with the *reduced* unbinding probability ε_o/q, where the interaction parameter $q>1$ describes an effectively attractive interaction between two motors from the same species. If it is behind a minus motor, it unbinds with the *enhanced* unbinding probability $\varepsilon_o q$; and (b) sticking probabilities for plus motor particles (not shown) which attempt to bind to an empty filament site. If the plus motor attempts to bind to a site behind a bound plus or minus motor, the sticking probability is enhanced and reduced, and is given by $\pi_o q$ and π_o/q, respectively. The same unbinding and sticking probabilities apply if all plus motors shown here are transformed into minus motors and vice versa [61].

effectively attractive interaction between two motors of the same species, we have $q>1$. In the presence of a bound motor of the other species at the forward neighbor site the unbinding rate is enhanced by a factor q, while the adsorption rate is reduced by a factor $1/q$, see Fig. 19.

6.3.5. *Phase transitions between different steady states*

For $q=1$, the system defined in the previous system corresponds to motor particles which interact only via their mutual exclusion or hard core repulsion. As one increases the interaction parameter q, one finds new system behavior corresponding to a phase transition with spontaneous symmetry breaking. Thus, the system is now characterized by a critical value q_c for the interaction parameter q, and qualitatively different behavior for $q<q_c$ and $q>q_c$. An example for this behavior is shown in Fig. 20. Inspection of this figure shows that both the order parameter m_b and the current J_b exhibit a hysteresis loop for $q>q_c$ which corresponds to a discontinuous phase transition.

In the presence of the effectively attractive interactions, the two relations of radial detailed balance become q-dependent and have the form [61]

$$\begin{aligned} &-\varepsilon\rho_{b,\pm}(1-\rho_{ub})\left[(1-\rho_b)+q\rho_{b,\mp}+\frac{1}{q}\rho_{b,\pm}\right] \\ &\quad=\pi_{ad}\rho_{ub,\pm}(1-\rho_b)\left[(1-\rho_b)+\frac{1}{q}\rho_{b,\mp}+q\rho_{b,\pm}\right] \end{aligned} \tag{6.26}$$

within mean field theory with $\varepsilon=3\varepsilon_o/2$ and the various densities as defined before.

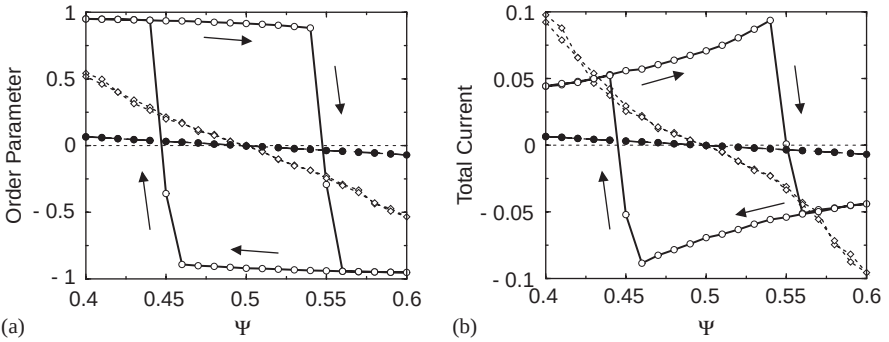

Fig. 20. (a) Order parameter $m_b = \rho_{b,+} - \rho_{b,-}$ and (b) total current $J_b = J_{b,+} + J_{b,-}$ as a function of the relative mole fraction Ψ of the two species of motor particles. Three sets of Monte Carlo data are shown: the full circles, open diamonds, and open circles correspond to interaction parameter $q = 1$ (hard core interaction only), $q = 6$, and $q = 15$, respectively. The critical point of this system is at $q = q_c \simeq 7.9$. Both for $q = 1$ and $q = 6 < q_c$, the order parameter and the total current decrease smoothly with increasing Ψ. In contrast, for $q = 15 > q_c$, these two quantities exhibit a large hysteresis loop corresponding to a discontinuous phase transition. The data for $q = 6$ are relatively noisy which indicates the onset of critical fluctuations.

Now, consider the symmetric case in which the number of plus and minus motor particles is equal, i.e., $N_- = N_+$. In the limit of large tube radius R, this implies $\rho_{ub,+} = \rho_{ub,-} = \rho_{ub}/2$ irrespective of the behavior of the bound motors. In this case, the relation (6.26) leads to two equations which can be solved for the bound motor densities $\rho_{b,+}$ and $\rho_{b,-}$ as functions of unbound motor density ρ_{ub}, interaction parameter q, and probability ratio ε/π_{ad}. This solution undergoes a continuous bifurcation at the critical value [61]

$$q_c \equiv \eta + \sqrt{\eta^2 + 3} \quad \text{with } \eta \equiv \frac{\varepsilon}{\pi_{ad}} \frac{1 - \rho_{ub}}{\rho_{ub}} \,. \tag{6.27}$$

of the interaction parameter as shown in Fig. 21, which implies that the symmetric system with an equal number of plus and minus motor particles undergoes a continuous phase transition within mean field theory. The existence of such a transition has been confirmed by Monte Carlo simulations [61]. For the parameter values $\varepsilon = 0.01$, $\pi_{ad} = 0.1$, and $\rho_{ub} = 0.1$, mean field theory leads to the critical interaction parameter $q_c = 2.83$ as follows from (6.27). The Monte Carlo simulations lead to the estimate $q_c \simeq 7.9$ for the same set of parameters which shows that the mean field value of q_c is strongly increased by fluctuations.

The order parameter $m_b = \rho_{b,+} - \rho_{b,-}$ vanishes for $q < q_c$, but attains a finite value for $q > q_c$ which scales as $m_b \sim \pm(q - q_c)^{1/2}$ close to the transition point. The Monte Carlo simulations in Ref. [61] lead to

$$m_b \sim \pm(q - q_c)^{\beta} \quad \text{with } \beta \simeq 0.35 \,. \tag{6.28}$$

Likewise, the total current J_b behaves as

$$J_b \sim \pm(q - q_c)^{\chi} \,. \tag{6.29}$$

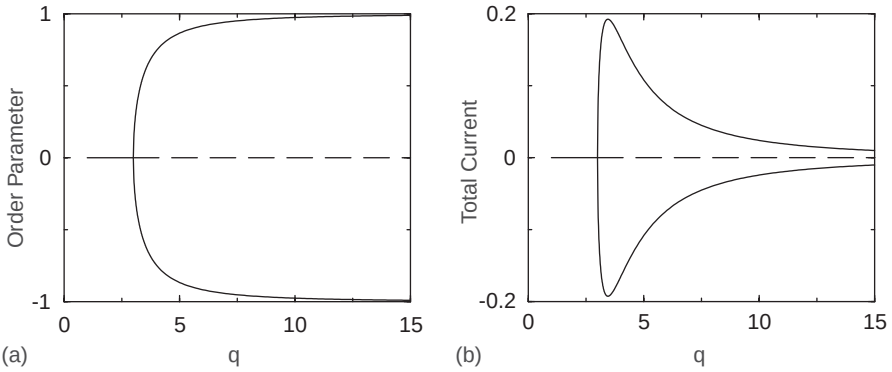

Fig. 21. (a) Order parameter $m_b = \rho_{b,+} - \rho_{b,-}$ and (b) total current $J_b = J_{b,+} + J_{b,-}$ as a function of the interaction parameter q for the symmetric case with an equal number of plus and minus motor particles as obtained within mean field theory. The system exhibits the critical interaction parameter $q = q_c$ at which both order parameter and total current vanish in a continuous fashion. As one moves further into the steady state with broken symmetry, the order parameter increases continuously whereas the total current exhibits again a maximum arising from the formation of traffic jams [61].

Since the current is related to the order parameter via $J_b = v_b m_b(1 - \rho_{ub})$ within mean field theory, this theory predicts the scaling relation $\chi = \beta$ and the mean field value $\chi = 1/2$. As one increases the interaction parameter q above $q = q_c$, the system moves further into the steady state with broken symmetry, and the order parameter increases continuously. In contrast, the total current exhibits again a maximum arising from the formation of traffic jams for large values of q, see Fig. 21(b).

In systems with several parallel filaments, the symmetry breaking leads to the coexistence of traffic lanes with opposite directionality. This behavior is already observable for a tubular compartment which contains two parallel filaments with the same orientation as shown in Fig. 22. The system contains again the same number of plus and minus motor particles. If one motor species starts to occupy one filament, the other motor species attains a larger bulk concentration and is, thus, more likely to bind to the other filament. Indeed, for $q > q_c$, the two filaments are covered by different motor species which then form two traffic lanes with opposite directionality. Thus, the symmetry breaking provides a simple mechanism for efficient transport between two reservoirs of cargo particles.

In Fig. 22, the minus motor particles occupy filament (1) whereas the plus motor particles occupy filament (2). If the system has a finite volume, the state shown in Fig. 22 corresponds to a quasi-steady state. Indeed, for a finite system, the fluctuations in the motor particle densities will lead, once in a while, to another quasi-steady state in which the plus motor particles occupy filament (1) and the minus motor particles occupy filament (2). The time scale which governs the transitions between these two quasi-steady states diverges in the limit of large system volume.

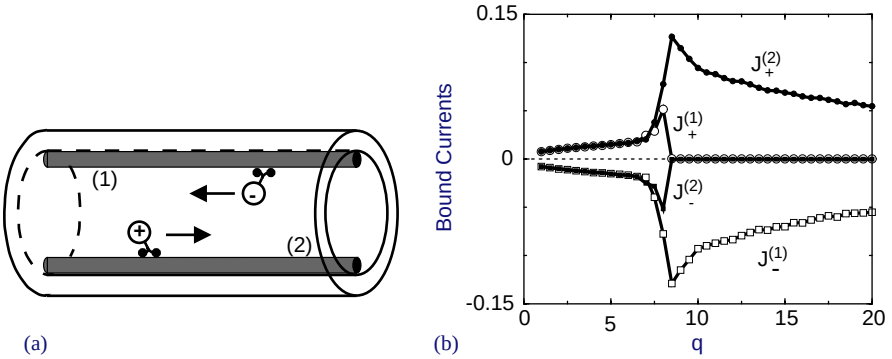

Fig. 22. (a) Tubular compartment with two parallel filaments (1) and (2), which have the same orientation, and with an equal number of plus and minus motor particles. For $q > q_c$, the symmetry of the system is spontaneously broken and one obtains a quasi-steady state in which one filament is occupied by plus motor particles, the other by minus ones. (b) Different bound currents for the steady state shown in (a) as a function of the interaction parameter q. The plus motor particles generate the bound currents $J_+^{(1)}$ and $J_+^{(2)}$ on filament (1) and (2), respectively; likewise, the minus motor particles generate the currents $J_-^{(1)}$ and $J_-^{(2)}$. Close to the critical value $q = q_c$ of the interaction parameter, both types of motors walk on both filaments.

7. Self-organization in biomimetic nanosystems

This article has discussed various aspects of the movements of molecular motors and motor particles which involve many length and time scales. In systems with many interacting motor particles, our theory predicts a variety of cooperative phenomena and self-organized processes which should be accessible to experiments: build-up of traffic jams which strongly affect the transport properties of these systems; active structure formation leading to steady states with nonuniform density and current patterns; phase transitions between two different steady states in systems with a single motor species in contact with motor particle reservoirs; phase transitions between two different steady states in systems with two species of molecular motors.

All of these phenomena and processes have been illustrated here for a particularly simple geometry: a tubular compartment with a single filament. It is quite obvious that these cooperative phenomena and self-organized processes are also present for more complex arrangements of the filaments. One example is provided by centered arrangement of filaments as discussed in Ref. [66]. Likewise, one may study more complex transport phenomena such as (i) motor transport along filaments with frozen defects or obstacles, see, e.g., Ref. [67], (ii) mutual transport of molecular motors which may be effective in axons, or (iii) motor transport of regulatory molecules which can locally change the motor activity.

The systems discussed here were characterized by the basic property that the motors were mobile but the filaments were immobilized. It is also possible to construct motor/filament systems for which the motors are immobilized and the filaments are mobile. The cooperative behavior of these latter systems remains to be

explored. On the other hand, more complex systems consisting of motor and filaments which are both mobile have already been studied to some extent both for kinesin/microtubule systems [68] and for myosin/F-actin systems [69].

The cytoskeletal motors discussed in this article are stepping motors which generate pulling forces. Indeed, these motors can pull various types of cargo such as vesicles. Filaments, on the other hand, can grow and then generate pushing forces. Various motility assays have been constructed by which these filaments push against a surface or colloidal particle. The growth of actin filaments can be site-directed by surface-anchored molecules. One assay contains surface-anchored WASP proteins which recruit Arp2/3 protein complexes and G-actin monomers to the surface in order to initiate the growth of branched bundles of actin filaments [70]. More recently, surface-anchored formin proteins has been shown to initiate the growth of unbranched actin bundles [71]. Microtubules have been grown in vesicles [72], and growing microtubules have been shown to buckle when they grow against a solid obstacle [73].

From the experimental point of view, active biomimetic systems provide many challenges such as (i) the construction of active transport systems for the sorting of biomolecules, (ii) transport systems which can be switched by externally applied

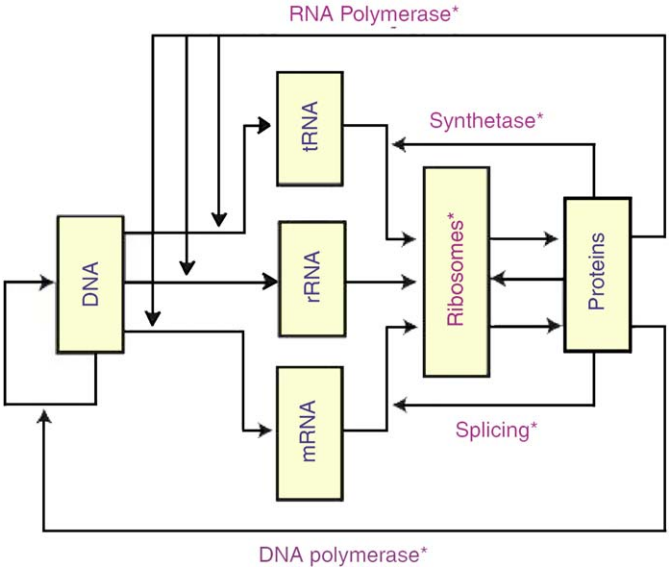

Fig. 23. Schematic view of the information processing network within the living cell which is based on DNA, various types of RNA, and proteins. The replication of DNA, the transcription of DNA into RNA, and the translation of RNA into proteins require the activity of different molecular motors or assemblers marked by an asterisk. All of these assemblers are themselves produced by these networks which implies that the network cannot be taken further apart and, thus, has a certain minimal complexity. The formation of the assembler complexes from proteins or proteins and RNA seems to occur spontaneously. For simplicity, additional feedback loops of regulation from proteins and RNA to transcription and translation have been omitted.

forces, (iii) site-directed growth of actin filaments in vesicles, or (iv) the construction of contractile myosin/actin bundles which would represent genuine 'nanomuscles'. All of these problems will be pursued in a forthcoming European network on 'Active Biomimetic Systems'.

Even though much has been achieved in the area of biomimetic nanosystems during the last decade, there is still a large gap in complexity between the most advanced biomimetic systems and simple unicellular organisms. Even the most primitive organisms contain rather complex networks of different types of biomolecules. One particularly intriguing example is provided by the information processing networks which consist of DNA, RNA, and proteins, as shown in Fig. 23. The flow of information from DNA to RNA to proteins, which is primarily based on transcription of DNA into RNA and on translation of RNA into proteins, requires the activity of several molecular motors or machines; in Fig. 23, these motors are indicated by an asterisk. It is rather remarkable that the assembly of these motors is also based on the same information processing networks. In this sense, these networks are circular and entangled and it is difficult to see how they may have evolved in nature or how one might build them up from simpler building blocks.

Acknowledgements

We thank Nicole Jaster and Theo Nieuwenhuizen for enjoyable collaborations and acknowledge support by the Human Frontier Science Project.

Appendix A. Driven Brownian ratchets

The general Brownian ratchets described in this appendix were introduced and studied in Refs. [28–32] and represent extensions of the Smoluchowski or Fokker–Planck equation as given by (3.2)–(3.4). The movement of the motor along the filament is again described by a spatial coordinate, x. For cytoskeletal and other linear motors, one useful choice for x is the displacement of the center-of-mass of the motor parallel to the filament. For rotary motors, the variable x may represent an appropriate angular coordinate. In addition, for a given value of x, the motor can attain several internal states which are labeled by the discrete index m with $m = 1, 2, \ldots, M$.

A.1. Time evolution of probability distribution

The stochastic dynamics of the molecular motor is now described by the probability densities $P_m(x, t)$ to find the motor at position x and in internal state m. For a given position x, the densities P_m may change (i) because of lateral diffusion in state m which leads to lateral currents J_m or (ii) because of transitions between the different internal states. Therefore, the probability densities P_m satisfy the continuity

equations

$$\partial P_m(x,t)/\partial t + \partial J_m(x,t)/\partial x = I_m(x,t) \tag{A.1}$$

with the transition current densities I_m. In order to discuss these equations, it will be convenient to visualize the M internal states as M levels. In the following, the terms 'internal state' and 'level' are synonymous.

The lateral current J_m depends on the molecular interaction potential $U_m(x)$ between the motor in internal state m and the filament. The corresponding reduced potentials are defined by

$$V_m(x) \equiv U_m(x)/T \quad \text{for } m = 1, 2, \ldots, M\,. \tag{A.2}$$

We will assume that the x-dependence of the molecular interaction potentials $U_m(x)$ exhibits a characteristic length scale corresponding to the size of a single step ℓ along the filament. It will also be convenient to consider periodic potential with $U_m(x+\ell) = U_m(x)$.

Using the effective force potentials defined by (A.2), the lateral currents J_m have the Smoluchowski– or Fokker–Planck form [19,74]

$$J_m(x,t) \equiv -D_m \left[\frac{\partial}{\partial x} V_m(x) + \frac{\partial}{\partial x}\right] P_m(x,t)\,, \tag{A.3}$$

where the parameter D_m represents the small-scale diffusion coefficient for level m. The corresponding friction coefficients are given by T/D_m as follows from the Einstein relation.

The transition current densities I_m depend on the transition rate functions $\Omega_{mn} = \Omega_{mn}(x) \geqslant 0$ from state m to state n and have the generic form

$$I_m(x,t) \equiv \sum_n{}' \left[-P_m(x,t)\Omega_{mn}(x) + P_n(x,t)\Omega_{nm}(x)\right], \tag{A.4}$$

where the prime at the summation sign indicates that n is restricted to $n \neq m$.

A.2. From ratchets to networks

The generalized ratchet models defined so far are rather general. It is now convenient to further specify the transition rate functions and to take these functions to be localized in space at the discrete set of positions $x = x_k$ with $k = 1, \ldots, K$ and $0 \leqslant x_1 < \cdots < x_K < \ell$. A convenient parametrization of such localized transition rate functions is given by [28,30]

$$\Omega_{mn}(x) \equiv \sum_k \omega_{mn}(x_k)\ell_\Omega \delta(x - x_k)\,, \tag{A.5}$$

where $\omega_{mn}(x_k) \geqslant 0$ define the transition rates from level m to level n, $\ell_\Omega \ll \ell$ represents a molecular 'localization' length, and $\delta(z)$ is Dirac's delta function.

Using the parametrization (A.5) for the transition rate functions, these generalized ratchet models can be mapped onto stochastic networks consisting of MK discrete states or vertices (k,m), compare Fig. 5 [30,31]. In the steady state, the time-independent probabilities $P^{\rm st}(k,m)$ to find the motor in state (k,m) which are related

to the original probabilities $P_m^{\rm st}(x_k)$ via

$$P^{\rm st}(k,m) \equiv P_m^{\rm st}(x_k)\ell_\Omega \tag{A.6}$$

satisfy the steady-state master equation

$$\begin{aligned} 0 = \sum_n{}' & [-P^{\rm st}(k,m)W(k,m|k,n) + P^{\rm st}(k,n)W(k,n|k,m)] \\ & - P^{\rm st}(k,m)W(k,m|k+1,m) + P^{\rm st}(k+1,m)W(k+1,m|k,m) \\ & - P^{\rm st}(k,m)W(k,m|k-1,m) + P^{\rm st}(k-1,m)W(k-1,m|k,m)\,. \end{aligned} \tag{A.7}$$

with the 'vertical' transition rates

$$W(k,m|k,n) \equiv \omega_{mn}(x_k)\,, \tag{A.8}$$

where the prime at the summation sign indicates $n \neq m$.

The corresponding network is shown in Fig. 5. As indicated in this figure, the network satisfies periodic boundary conditions along the x-direction, which corresponds to the spatial displacement of the motor molecule, and has an arbitrary number of transverse dimensions. As far as the corresponding stochastic dynamics is concerned, the probability currents are conserved at each vertex.

Appendix B. Driven Brownian networks

In this subsection, we consider a network of possible motor states which are represented by the vertices i of the corresponding graph. The motor can undergo transitions from state i to state j with transition rates ω_{ij}; the corresponding directed edge or di-edge of the graph will be denoted by $\langle ij\rangle$. The probability $P_i(t)$ to find the motor in conformation i now satisfies the master equation

$$\partial P_i(t)/\partial t = \sum_j{}' \left(P_j(t)\,\omega_{ji} - P_i(t)\,\omega_{ij}\right), \tag{B.1}$$

where the prime indicates that the summation is restricted to $j \neq i$.

In the steady state, the time-independent probabilities $P_i = P_i^{\rm st}$ satisfy the relationships

$$0 = \sum_j{}' \left(P_i^{\rm st}\,\omega_{ij} - P_j^{\rm st}\,\omega_{ji}\right). \tag{B.2}$$

This equation can be solved using a graph theoretic method which was introduced by Kirchhoff in the context of electric circuits [75] and has been rederived in a variety of contexts [76–79]. The Kirchhoff method is also discussed in textbooks on graph theory, see, e.g., Refs. [80,81].

B.1. Graph theoretic solution for steady states

The network graph, $\mathcal{G}$, is taken to have $N_{\rm v}$ vertices and $N_{\rm e}$ (nondirected) edges. Each edge represents two directed edges or di-edges. Thus, if i and j are two vertices

which are connected by an edge, the di-edge $\langle ij\rangle$ points from i to j, whereas the di-edge $\langle ji\rangle$ points from j to i. By definition, the di-edge points towards its head vertex and away from its tail vertex. In general, a cycle $\mathscr{C}$ of any graph is a subgraph which consists of a closed walk, i.e., of an alternating sequence of vertices and (nondirected) edges between those vertices where each vertex and each edge occurs only once. For the networks considered here, it will be convenient to define directed cycles or di-cycles. Such a di-cycle consists of an alternating sequence of vertices and di-edges where every vertex is the head of precisely one di-edge and the tail of one other di-edge. If we replace the di-edges of a di-cycle by the corresponding (nondirected) edges, the di-cycle becomes a cycle. Therefore, each cycle $\mathscr{C}$ corresponds to two directed cycles or di-cycles $\mathscr{C}^+$ and $\mathscr{C}^-$ with opposite orientations.

A spanning tree, $\mathscr{T}_n$, of the network graph $\mathscr{G}$ contains all vertices but no cycles which implies that it has $N_v - 1$ (nondirected) edges. In general, there are many different spanning trees which will be distinguished by the index n with $n = 1, 2, \ldots, N_{\mathscr{T}}$, where $N_{\mathscr{T}}$ denoted the total number of spanning trees. From each spanning tree $\mathscr{T}_n$, one can construct an aborescence, $\mathscr{A}_{n,i}$, [80] which converges on the vertex i and which is obtained from the spanning tree by the following assignment of directions: (i) all edges are directed in such a way that all vertices are connected to either one or no outgoing di-edge; and (ii) the only vertex which is not connected to any outgoing di-edge is the vertex i. This procedure can be applied for each vertex i of each spanning tree $\mathscr{T}_n$ which implies that one has $N_{\mathscr{T}} N_v$ different aborescences.

For each aborescence $\mathscr{A}_{n,i}$, one can define the transition rate product

$$\Omega(\mathscr{A}_{n,i}) \equiv \prod_{\langle ab\rangle} \omega_{ab} \,, \tag{B.3}$$

where the product includes all di-edges $\langle ab\rangle$ contained in the aborescence $\mathscr{A}_{n,i}$. Since each aborescence has $N_v - 1$ di-edges, the product contains the same number of transition rates. Summation over all spanning trees for fixed vertex i defines the sum

$$\Omega_i \equiv \sum_n \Omega(\mathscr{A}_{n,i}) \,, \tag{B.4}$$

and a final summation over all vertices leads to the normalization factor

$$\Omega \equiv \sum_i \Omega_i = \sum_i \sum_n \Omega(\mathscr{A}_{n,i}). \tag{B.5}$$

The steady-state distribution which satisfies the time-independent master equation (B.2) is now simply given by

$$P_i^{\mathrm{st}} = \Omega_i / \Omega \,. \tag{B.6}$$

Note that both Ω_i and Ω are *multilinear* in all transition rates ω_{ij} which implies that the steady-state distributions P_i^{st} correspond to ratios of two multilinear polynomials.

In order to characterize the steady state, one needs to determine the currents in addition to the probabilities. The excess currents, $\Delta J_{ij}^{\rm st}$, through the di-edges $\langle ij\rangle$ are given by

$$\Delta J_{ij}^{\rm st} \equiv P_i^{\rm st}\,\omega_{ij} - P_j^{\rm st}\,\omega_{ji} = \tfrac{1}{\Omega}[\Omega_i\omega_{ij} - \Omega_j\omega_{ji}]\,. \tag{B.7}$$

In this way, the excess currents are also expressed as ratios of two polynomials which are multilinear in all transition rates.

Apart from the normalization factor $1/\Omega$, the excess currents $\Delta J_{ij}^{\rm st}$ are given by the differences $[\Omega_i\omega_{ij} - \Omega_j\omega_{ji}]$ which can be expressed in terms of subgraphs. In fact, many terms cancel in the difference, and those terms, which survive after the cancellation, can be identified with all spanning subgraphs of $\mathscr{G}$ which *contain exactly one cycle and for which this cycle goes through the edge between i and j*. As previously mentioned, each cycle $\mathscr{C}$ corresponds to two di-cycles $\mathscr{C}^+$ and $\mathscr{C}^-$ with opposite orientation.

Now, let us define di-cycles $\mathscr{C}_{ij,k}^+$ and $\mathscr{C}_{ij,k}^-$ which contain the di-edge $\langle ij\rangle$ and $\langle ji\rangle$, respectively. The index k indicates that there can be several such di-cycles. By definition, one has $\mathscr{C}_{ij,k}^- = \mathscr{C}_{ji,k}^+$, i.e., if one changes the orientation of $\mathscr{C}_{ij,k}^+$, one obtains the di-cycle $\mathscr{C}_{ji,k}^+$ through the di-edge $\langle ji\rangle$. The corresponding transition rate products will be denoted by

$$\Omega(\mathscr{C}_{ij,k}^+) \equiv \prod_{\langle ab\rangle} \omega_{ab} \quad \text{and} \quad \Omega(\mathscr{C}_{ij,k}^-) = \Omega(\mathscr{C}_{ji,k}^+) \equiv \prod_{\langle ba\rangle} \omega_{ba}\,, \tag{B.8}$$

where the products include all di-edges of the corresponding di-cycles.

The (nondirected) cycle $\mathscr{C}_{ij,k}$ is obtained from either $\mathscr{C}_{ij,k}^+$ or $\mathscr{C}_{ij,k}^-$ by replacing all di-edges by the corresponding (nondirected) edges. In general, the cycles $\mathscr{C}_{ij,k}$ do not contain all $N_{\rm v}$ vertices of the network graph but only a subset of them. In order to convert these cycles into spanning subgraphs without creating more cycles, one has to 'attach' a sufficient number of tree-like side branches to them; the resulting subgraphs will be denoted by $\mathscr{B}_{ij,k,l}$. The index l indicates that each cycle $\mathscr{C}_{ij,k}$ will, in general, lead to several spanning subgraphs $\mathscr{B}_{ij,k,l}$ which differ in their side branches. Each spanning subgraph $\mathscr{B}_{ij,k,l}$ defines two directed subgraphs $\mathscr{B}_{ij,k,l}^+$ and $\mathscr{B}_{ij,k,l}^-$, which are obtained by the following assignment of directions: (i) $\mathscr{B}_{ij,k,l}^+$ contains the di-cycle $\mathscr{C}_{ij,k}^+$ whereas $\mathscr{B}_{ij,k,l}^-$ contains the di-cycle $\mathscr{C}_{ij,k}^-$; and (ii) all side branches are oriented towards the cycle $\mathscr{C}_{ij,k}$.

Each 'decorated' di-cycle $\mathscr{B}_{ij,k,l}^+$ has $N_{\rm v}$ vertices and $N_{\rm e}$ edges and leads to the transition rate product

$$\Omega(\mathscr{B}_{ij,k,l}^+) \equiv \prod_{\langle ab\rangle} \omega_{ab} = \Omega(\mathscr{C}_{ij,k}^+) \prod_{\langle a'b'\rangle} \omega_{a'b'}\,, \tag{B.9}$$

where the first product consists of $N_{\rm v}$ transition rates corresponding to all di-edges $\langle ab\rangle$ contained in $\mathscr{B}_{ij,k,l}^+$ and the second product corresponds to all di-edges $\langle a'b'\rangle$ contained in the side branches.

When expressed in terms of these transition rate products, the excess currents defined in (B.7) have the general form

$$\Delta J_{ij}^{\rm st} = \frac{1}{\Omega} \sum_{k,l} [\Omega(\mathscr{B}_{ij,k,l}^+) - \Omega(\mathscr{B}_{ij,k,l}^-)]\,, \tag{B.10}$$

where the k-summation runs over all di-cycles, which contain the di-edge $\langle ij\rangle$, and the l-summation runs over all possible ways to 'decorate' a given di-cycle with tree-like side branches and, thus, to convert it into a spanning subgraph. Using the factorization property (B.9), one finally obtains the expression

$$\Delta J_{ij}^{\mathrm{st}} = \frac{1}{\Omega}\sum_{k}\left([\Omega(\mathscr{C}_{ij,k}^{+}) - \Omega(\mathscr{C}_{ij,k}^{-})] \sum_{l} \prod_{\langle a'b'\rangle} \omega_{a'b'} \right) . \tag{B.11}$$

Each term which contributes to the excess current $\Delta J_{ij}^{\mathrm{st}}$ in (B.11) is proportional to

$$\Delta\Omega_{ij,k} \equiv \Omega(\mathscr{C}_{ij,k}^{+}) - \Omega(\mathscr{C}_{ji,k}^{-}) = \prod_{\langle ab\rangle} \omega_{ab} - \prod_{\langle ba\rangle} \omega_{ba} , \tag{B.12}$$

i.e., to the difference in the transition rate products for the two di-cycles $\mathscr{C}_{ij,n}^{+}$ and $\mathscr{C}_{ij,n}^{-}$ which differ only in their orientation. In this sense, the expression (B.11) for the excess current $\Delta J_{ij}^{\mathrm{st}}$ represents a *decomposition into all cycles* which contain the (nondirected) edge between i and j.

B.2. Some simple examples

A rather simple example is obtained if one studies a network consisting of a single cycle as the one displayed in the left part of Fig. 6. This single cycle is now denoted by $\mathscr{C}_{ij,1}$ and is taken to have $N_{\mathrm{v}} = K$ vertices and $N_{\mathrm{e}} = K$ edges. The vertices are labeled by $i = 1, 2, \ldots, K$. Using the general expression (B.11), the excess current through the di-edge $\langle 12\rangle$ is found to be

$$\Delta J_{12}^{\mathrm{st}} = \frac{\Delta\Omega_{12,1}}{\Omega} = \frac{1}{\Omega}(\omega_{12}\,\omega_{23}\ldots\omega_{K1} - \omega_{1K}\ldots\omega_{32}\,\omega_{21}) , \tag{B.13}$$

where Ω is defined by (B.5) and consists of terms with $K-1$ transition rate factors. All other edges of the cycle have the same excess current, i.e., $\Delta J_{12}^{\mathrm{st}} = \Delta J_{23}^{\mathrm{st}} = \cdots = \Delta J_{K1}^{\mathrm{st}}$.

A rather similar expression for the excess current is obtained for a network which consists of a single cycle with tree-like side branches. The cycle has again K vertices and edges, whereas the total number of the vertices N_{v} and the total number of edges N_{e} satisfy $N_{\mathrm{v}} = N_{\mathrm{e}} > K$. The vertices of the cycle are again labeled by $i = 1, 2, \ldots, K$. In this case, the excess current for the di-edge $\langle 12\rangle$ is given by

$$\Delta J_{12}^{\mathrm{st}} = \frac{\Delta\Omega_{12,1}}{\Omega}\prod_{\langle a'b'\rangle}\omega_{a'b'} = \frac{1}{\Omega}(\omega_{12}\,\omega_{23}\ldots\omega_{K1} - \omega_{1K}\ldots\omega_{32}\omega_{21})\prod_{\langle a'b'\rangle}\omega_{a'b'} , \tag{B.14}$$

where the latter product runs over all di-edges $\langle a'b'\rangle$ contained in the tree-like side branches. Again, all other edges of the cycle have the same excess current as $\langle 12\rangle$ whereas all edges within the tree-like side branches have zero excess current.

The excess currents through the cycle edges as given by (B.13) and (B.14) vanish if $\omega_{12}\,\omega_{23}\ldots\omega_{K1} = \omega_{1K}\ldots\omega_{32}\,\omega_{21}$. This latter equality can be fulfilled for various choices of the transition rates: (i) all rates of the cycle are equal, i.e., $\omega_{ij} = \omega_{ji} = \omega$;

(ii) backward and forward rates of the cycle are pairwise equal, i.e., $\omega_{ij} = \omega_{ji}$; or (iii) $2K-1$ rates of the cycle are arbitrary (and nonzero) and the $2K$th rate, say ω_{12}, is given by $\omega_{12} = \omega_{1K} \ldots \omega_{32}\omega_{21}/\omega_{23} \ldots \omega_{K1}$.

A nonzero current for the 1-cycle network is obtained, e.g., if all rates are equal to ω apart from the forward and backward rates $\omega_{12} = \omega + \delta$ and $\omega_{21} = \omega + \delta'$ between the vertices 1 and 2 of the cycle. This leads to the current

$$\Delta J_{12}^{\mathrm{st}} = \frac{\omega(\delta - \delta')}{N_{\mathrm{v}} K\omega + N_{\mathrm{v}}(K-1)(\delta + \delta')/2} \tag{B.15}$$

with $\Delta J_{12}^{\mathrm{st}} = \Delta J_{23}^{\mathrm{st}} = \cdots = \Delta J_{K1}^{\mathrm{st}}$ and $\Delta J_{ab}^{\mathrm{st}} = 0$ for all di-edges $\langle ab \rangle$ of the tree-like side branches.

Another relatively simple network contains a disjoint set of M cycles which are connected either by a single vertex, a single edge, or a tree-like subgraph. Furthermore, if we contract all edges which belong to a cycle, we obtain a tree. Such a network represents 'a tree of cycles'. For such a network, each cycle can carry a different current, and the excess currents $\Delta J_{ij}^{\mathrm{st}} \neq 0$ if the di-edge $\langle ij \rangle$ belongs to one of those cycles, $\mathscr{C}_{ij,k}$. Each of these latter currents is proportional to the excess quantity $\Delta\Omega_{ij,k}$ as defined in (B.12).

The situation becomes more complex as soon as one has pairs of cycles which have joint edges, pairs of cycles which are connected by several edges, or more than two cycles which form cyclic chains. However, it is still possible, at least in principle, to determine all possible cycles of a given network by the systematic procedure explained in the next subsection.

B.3. Finite vector space of cycles

All (nondirected) cycles $\mathscr{C}$ of an arbitrary graph form a finite vector space over the finite field $\{0, 1\}$, see, e.g., Ref. [82]. The vector addition, $\mathscr{C}_1 + \mathscr{C}_2$, of two cycles $\mathscr{C}_1$ and $\mathscr{C}_2$ corresponds to the operation of symmetric difference applied to the edge sets of these cycles. In general, the symmetric difference of two sets X and Y is defined by $X + Y \equiv (X \cup Y) \backslash (X \cap Y)$.

A fundamental set of (nondirected) cycles, which provides a basis for the finite vector space of cycles, can be constructed starting from an arbitrary spanning tree $\mathscr{T}_n$ of the network graph $\mathscr{G}$. Such a tree has $N_{\mathrm{v}} - 1$ edges and $N_{\mathrm{ch}} \equiv N_{\mathrm{e}} - N_{\mathrm{v}} + 1$ chords which are those edges of $\mathscr{G}$ which do not belong to $\mathscr{T}_n$. If one adds one chord to the spanning tree $\mathscr{T}_n$, one obtains a subgraph with exactly one cycle. In fact, each chord leads to a different cycle, and the set of N_{ch} cycles, which are generated in this way, provides a fundamental set. All other cycles and all disjoint unions of cycles can be generated by vector addition of these fundamental cycles. Thus, the number of cycles and disjoint unions of cycles is given by $2^{N_{\mathrm{ch}}}$ which includes the empty set as the union of no cycles. Without this empty set, one has $2^{N_{\mathrm{ch}}} - 1$ different cycles and disjoint unions of cycles.

We now disregard all disjoint unions of cycles since they do not contribute to the cycle decomposition of the excess currents $\Delta J_{ij}^{\mathrm{st}}$ as given by (B.11). If the number of disjoint unions of cycles is denoted by N_{duc}, the number of cycles,

$N_{\rm cy}$, is given by

$$N_{\rm cy} = 2^{N_{\rm ch}} - 1 - N_{\rm duc} \,. \tag{B.16}$$

This is also the maximal number of k-values which can contribute in the expression (B.11) for the excess currents $\Delta J_{ij}^{\rm st}$.

B.4. Equilibrium and detailed balance

In equilibrium with $P_i^{\rm st} = P_i^{\rm eq}$, all excess currents $\Delta J_{ij}^{\rm st} = \Delta J_{ij}^{\rm eq}$ vanish for all edges of the network. The relation $\Delta J_{ij}^{\rm eq} = P_i^{\rm eq}\,\omega_{ij} - P_j^{\rm eq}\omega_{ji}$ then implies that the probability currents in the network are in *detailed balance*, i.e., the forward and the backward probability currents are equal and, thus, satisfy the $N_{\rm e}$ relations

$$P_i^{\rm eq}\omega_{ij} = P_j^{\rm eq}\omega_{ji} \tag{B.17}$$

for all edges of the network graph.

If the equilibrium probabilities $P_i^{\rm eq} \neq 0$ for all vertices i, the detailed balance relation (B.17) can be formulated in a slightly different manner by introducing the 'energy landscape'

$$E_i \equiv -\ln(P_i^{\rm eq}) + E_o \,, \tag{B.18}$$

where E_o follows from the normalization of $P_i^{\rm eq}$. The detailed balance relation (B.17) is then equivalent to

$$\exp(E_i - E_j) = \frac{\omega_{ij}}{\omega_{ji}} \tag{B.19}$$

for all edges. Note that the energy landscape E_i remains unchanged if we replace the forward and backward transition rate constants ω_{ij} and ω_{ji} by $\tau(ij)\,\omega_{ij}$ and $\tau(ij)\,\omega_{ji}$, respectively, where $\tau(ij)$ represents an arbitrary function on the set of edges. In this way, one can define many different stochastic processes which all lead to the same equilibrium distribution.

Now consider any di-cycle $\mathscr{C}$ with K edges and perform K iterations of the detailed balance relation $P_j^{\rm eq} = (\omega_{ij}/\omega_{ji})P_i^{\rm eq}$ until the full di-cycle has been completed. The final probability must then be equal to the starting one, which implies that

$$\prod_{\langle ij\rangle} \frac{\omega_{ij}}{\omega_{ji}} = 1 \quad \text{or} \quad \prod_{\langle ij\rangle} \omega_{ij} = \prod_{\langle ji\rangle} \omega_{ji} \ \text{ for any cycle } \mathscr{C} \tag{B.20}$$

which is equivalent to

$$\sum_{\langle ij\rangle} (E_i - E_j) = 0 \quad \text{for any } \mathscr{C} \,. \tag{B.21}$$

Since these latter relations follow from the detailed balance equations (B.17) and (B.19), they represent necessary conditions for these equations to hold. In fact, they are also sufficient as follows from the explicit solution (B.11) for the excess currents $\Delta J_{ij}^{\rm st}$. Indeed, if the relation (B.20) is fulfilled for all cycles $\mathscr{C}$, we conclude from (B.11) that all excess currents vanish.

For a given stochastic network, the global relations as given by (B.20) can be checked without explicitly solving the master equation. In fact, it is not necessary to check these relations for all cycles but only for a fundamental set of cycles. Indeed, if (B.20) is valid for two cycles $\mathscr{C}_1$ and $\mathscr{C}_2$, it is also valid for $\mathscr{C}_1 + \mathscr{C}_2$ where the plus sign corresponds to the symmetric difference of the edge sets of the two cycles as explained above.

Thus, the N_e detailed balance relations $P_i^{eq}\,\omega_{ij} = P_j^{eq}\,\omega_{ji}$ as given by (B.17) are equivalent to the $N_{ch} = N_e - N_v + 1$ relations

$$\prod_{\langle ij\rangle} \omega_{ij} = \prod_{\langle ji\rangle} \omega_{ji} \quad \text{for all cycles } \mathscr{C}_f \tag{B.22}$$

which belong to a fundamental set of cycles. In this form, the detailed balance relations are no longer local but have the advantage that they are expressed only in terms of the transition rates which are considered to be the basic parameters of the network.

Appendix C. Parameter mapping for motor walks

In this appendix, we describe the parameter mapping for the motor walks of noninteracting motor particles. The first mapping introduced in Ref. [40] uses two different time scales for the bound and unbound state of the motor particles and is explained in the first subsections C.1–C.4. We also used a simplified mapping [41,42] which is based on a single time scale and described in the last subsection C.5 below.

C.1. Time scales for bound motors

The bound movement of a single motor particle exhibits several time scales. The basic time scale, τ_b, is taken to be the stepping time of a single molecular motor which is the average time for a forward step of this motor molecule. For two-headed kinesin, recent experiments indicate that this stepping time is 70 μs or smaller [6].

The dwell time, τ_{dw}, of the bound motor particle is the average time during which it remains bound to a certain filament position without stepping forward (or backward). This dwell time increases with decreasing ATP concentration since the ATP molecules have to diffuse to the ATP adsorption domains of the motor heads. For two-headed kinesins, this time scale becomes of the order of seconds for ATP concentrations in the μM regime. As one increases the ATP concentration, the dwell time decreases and reaches a constant saturation value which reflects the intrinsic time scale of the motor cycle. For two-headed kinesin, this saturation concentration is of the order of 1 mM ATP.

The cycle time, τ_{cy}, of a single stepping motor consists of the sum of its dwell and its stepping time, i.e.,

$$\tau_{cy} = \tau_{dw} + \tau_b\,. \tag{C.1}$$

The three time scales τ_b, τ_{dw}, and τ_{cy} are determined by the molecular dynamics of a single step.

In contrast, the walking time Δt_b of a motor particle follows from the statistics of many motor steps. This latter time scale represents the average time over which this particle remains bound to the filament. Two-headed kinesin, e.g., makes of the order of 100 steps before it unbinds from the filament. If N_{st} is the mean number of steps in the bound state, one has $\Delta t_b = N_{st}\tau_{cy}$.

C.2. Parameter mapping for bound motor particles

In the lattice models, the bound motor particle undergoes a discrete random walk at discrete time steps $t_n \equiv n\tau_b$. At each time step, the motor particle can make a forward or backward step to a neighboring binding site of the filament with hopping probability α and β, respectively. In addition, it can simply stay at the same binding site with probability γ or unbind from the filament with probability ε_o. These probabilities are normalized via

$$\alpha + \beta + \gamma + \varepsilon_o = 1 \,. \tag{C.2}$$

In terms of these probabilities and the basic scales ℓ and τ_b, one obtains the bound state velocity

$$v_b = (\bar{\alpha} - \bar{\beta})\,\frac{\ell}{\tau_b} \tag{C.3}$$

with the reduced hopping probabilities

$$\bar{\alpha} \equiv \alpha/(\alpha + \beta + \gamma) \quad \text{and} \quad \bar{\beta} \equiv \beta/(\alpha + \beta + \gamma)\,, \tag{C.4}$$

and the bound state diffusion coefficient

$$D_b = [\bar{\alpha} + \bar{\beta} - (\bar{\alpha} - \bar{\beta})^2]\,\frac{\ell^2}{2\tau_b} \,. \tag{C.5}$$

The bound state velocity and the bound state diffusion coefficient determine the randomness parameter, π_r, as considered, e.g., in Ref. [83]. When expressed in terms of the model parameters, the randomness parameter is given by

$$\pi_r \equiv \frac{2D_b}{\ell v_b} = \frac{\alpha + \beta}{\alpha - \beta} - \frac{\alpha - \beta}{\alpha + \beta + \gamma} \,. \tag{C.6}$$

The dwell probability γ determines the dwell time τ_{dw} of the motor particle via the relation

$$\tau_{dw} = \tau_b\gamma/(1 - \gamma) \tag{C.7}$$

and the cycle time

$$\tau_{cy} \equiv \tau_{dw} + \tau_b = \tau_b/(1 - \gamma)\,. \tag{C.8}$$

Likewise, the walking time, Δt_b, of the bound motor particle is related to the probability ε_o via

$$\Delta t_b = \tau_b \frac{1-\varepsilon_o}{\varepsilon_o} , \tag{C.9}$$

which implies the corresponding walking distance

$$\Delta x_b \equiv v_b \Delta t_b = \ell \frac{\alpha-\beta}{\varepsilon_o} \tag{C.10}$$

where the relation $\alpha+\beta+\gamma = 1-\varepsilon_o$ has been used.

It is straightforward to invert these relations, i.e., to express the model parameters in terms of measurable motor properties. As mentioned, the stepping time τ_b is, in principle, accessible to experimental observation. Furthermore, this time scale can be expressed as

$$\tau_b = \left(\frac{1+\zeta}{1-\zeta} - \pi_r\right)\frac{\ell}{v_b} \quad \text{with } \zeta \equiv \frac{\beta}{\alpha} = \frac{\bar{\beta}}{\bar{\alpha}} \tag{C.11}$$

and the randomness parameter π_r as given by (C.6). The parameter ζ represents the ratio of the backward and forward hopping probabilities; if backward steps are rare compared to forward steps, one has $\zeta \simeq 0$. The relation (C.11) expresses the stepping time τ_b in terms of ℓ, v_b, ζ, and π_r.

The relation (C.7) between the dwell probability γ and the dwell time τ_{dw} implies

$$\gamma = \frac{1}{1+\tau_b/\tau_{dw}} . \tag{C.12}$$

The relation (C.9) between the unbinding probability ε_o and the walking time Δt_b implies

$$\varepsilon_o = \frac{1}{1+\Delta t_b/\tau_b} . \tag{C.13}$$

It then follows from the relation (C.3) for the bound state velocity v_b that the forward and backward hopping probabilities, α and β, can be expressed as

$$\alpha = \frac{1}{2}\left[(1-\varepsilon_o)\left(1+\frac{\tau_b v_b}{\ell}\right) - \gamma\right] \tag{C.14}$$

and

$$\beta = \frac{1}{2}\left[(1-\varepsilon_o)\left(1-\frac{\tau_b v_b}{\ell}\right) - \gamma\right] . \tag{C.15}$$

Alternatively, one may also use the relation (C.10) for the walking distance Δx_b in order to obtain

$$\alpha = \frac{1}{2}\left[1+\frac{\Delta x_b}{\ell}\varepsilon_o - \varepsilon_o - \gamma\right] \tag{C.16}$$

and

$$\beta = \frac{1}{2}\left[1 - \frac{\Delta x_{\rm b}}{\ell}\varepsilon_o - \varepsilon_o - \gamma\right]. \tag{C.17}$$

C.3. Diffusion of unbound motor particles

So far, we have focussed on the parameters which determine the movement of the bound motor particle. After unbinding from the filament, the motor particle undergoes nondirected diffusive motion which can be characterized by the unbound diffusion coefficient $D_{\rm ub}$. This diffusion coefficient is related to the unbound friction coefficient $\phi_{\rm ub}$ via the Einstein relation

$$D_{\rm ub} = T/\phi_{\rm ub} \tag{C.18}$$

with temperature T (measured in energy units) where it has been implicitly assumed that the unbound diffusion does not involve any active processes.

In vitro, the motor diffuses in an aqueous solution which contains ions and ATP but behaves as a Newtonian fluid. In this case, the unbound friction coefficient $\phi_{\rm ub}$ is given by the Stokes friction coefficient

$$\phi_{\rm st} = 6\pi\eta R_{\rm hyd} \tag{C.19}$$

which depends on the dynamic viscosity η of the solution and on the effective hydrodynamic radius $R_{\rm hyd}$ of the motor particle. At room temperature, this leads to $D_{\rm ub} = (\eta_w/\eta) \times (100\,{\rm nm}/R_{\rm hyd}) \times 2.4\,\mu{\rm m}^2/{\rm s}$ with $\eta_w \simeq 0.9\,{\rm mPa\,s}$ ($\equiv$ cP) as appropriate for water. Thus, one has $D_{\rm ub} = 24\,\mu{\rm m}^2/{\rm s}$ for a motor molecule with a hydrodynamic radius of 10 nm, and $D_{\rm ub} = 2.4\,\mu{\rm m}^2/{\rm s}$ for a motor with an attached bead of radius 100 nm.

It is more difficult to estimate the diffusive motion of an unbound motor particle in vivo. The cytosol is densely packed and contains many macromolecules, supramolecular structures, and organelles, and the unbound motor particle may experience both repulsive and attractive interactions with these 'particles'. For repulsive interactions, these other particles represent additional steric barriers for the diffusive motion of the motor particle which will then exhibit a reduced diffusion coefficient. This reduction may be estimated by comparison with the diffusion of inert, electrically uncharged particles in fibroblasts for which the values $D_{\rm ub} \simeq 1.6\,\mu{\rm m}^2/{\rm s}$ and $\simeq 3 \times 10^{-3}\,\mu{\rm m}^2/{\rm s}$ have been measured for particle radii of 10 and 80 nm, respectively [84]. Compared to water, this corresponds to a size-dependent reduction factor of 10^{-1} and 10^{-3}, respectively. The Einstein relation (C.18) then implies that the unbound friction coefficient has increased by a factor of 10 and 10^3 for 10 and 80 nm particles, respectively. If the diffusing particle experiences attractive interactions, it will undergo diffusion in the presence of trapping sites and the overall motion will then be determined by the distribution of the corresponding trapping times. In addition, the precise value of the diffusion coefficient in living cells will depend on the type of these cell and on their cell cycle.

In general, one should expect that the diffusion coefficient $D_{\rm b}$ of the bound motor does not exceed the diffusion coefficient $D_{\rm ub}$ of the unbound one since the bound motor

experiences additional friction forces. The friction force for sliding the motor along the filament should be governed by the friction coefficient $\phi_{sl} = \phi_{ub} + \phi_{co}$, where ϕ_{co} arises from the contacts between motor particle and filament (if the surrounding medium is a Newtonian liquid, this sliding friction arising from Stokes flow in the presence of the filament). In addition, the walking motor has to undergo conformational changes which involve some internal molecular 'hinges'. The corresponding friction coefficient ϕ_{in} might be defined in such a way that the bound diffusion coefficient D_b satisfies

$$D_b \equiv T/(\phi_{sl} + \phi_{in}) = T/(\phi_{ub} + \phi_{co} + \phi_{in}) \,. \tag{C.20}$$

The intrinsic friction coefficient should depend on the activity of the motor and, thus, on the ATP concentration.

Comparison of (C.18) and (C.20) then implies that

$$D_b < D_{ub} \,. \tag{C.21}$$

This relation should hold in general, i.e., even if the friction forces are nonadditive.

The inequality (C.21) is confirmed by in vitro measurements for single kinesin motors. In this case, the bound diffusion coefficient was observed to be of the order of $10^{-3}\,\mu m^2/s$ [83,85] and $5 \times 10^{-2}\,\mu m^2/s$ [85] for two-headed and one-headed kinesin, respectively. Thus, for a normal aqueous solution, the unbound diffusion coefficient D_{ub} is much larger than the bound state diffusion coefficients D_b. In principle, one could reduce D_{ub} by a factor up to 10^{-2} if one changes the viscosity of the aqueous solution by adding some solutes such as glycerol or sucrose (provided these additional solutes do not suppress the catalytic activity of the molecular motors).

In vivo, the situation is different since the unbound diffusion coefficient is strongly reduced by the various particles in the cytosol as discussed above. A single kinesin motor attached to a 80 nm vesicle, e.g., should be characterized by an unbound diffusion coefficient $D_{ub} = T/\phi_{ub}$ which is reduced by a factor $\sim 10^{-3}$ compared to the in vitro case. On the other hand, the internal friction coefficient ϕ_{in} should be similar for in vivo and in vitro systems. In such a case, the friction of the bound motor particle may be dominated by the unbound friction coefficient ϕ_{ub} which implies that the two diffusion coefficients D_{ub} and D_b will then be of the same order of magnitude.

C.4. Parameter mapping for unbound motor particles

In the lattice models used here, the one-dimensional lattice of the filament with repeat distance ℓ is extended to a three-dimensional simple cubic lattice with lattice parameter ℓ. The unbound motor particles perform unbiased random walks on this lattice, i.e., each motor particle hops to one of the neighboring lattice sites with equal probability 1/6. This leads to the unbound diffusion coefficient

$$D_{ub} = \frac{1}{6}\frac{\ell^2}{\tau} \,, \tag{C.22}$$

where τ represents the basic time scale for the unbound motion.

In general, the time scale τ will be different from the basic time step τ_b for the bound motion. This difference has been explicitly taken into account in the Monte Carlo simulations in Ref. [40]. In this latter simulations, the motor particles were

taken to be single kinesin motors with two motor domains. The mapping of the different motor properties onto the lattice model as described in the previous subsections then leads to $\tau_b = 5.9\,\text{ms}$ and $\tau = \tau_b/1341 = 4.4\,\mu\text{s}$. It is not difficult to incorporate these two different time scales into the Monte Carlo simulations: the basic time scale is taken to be τ and one performs 1341 moves of unbound motor particles before one performs one move of a bound motor particle. Even though this procedure is straightforward, it is rather time consuming and we have also used the following simplified mapping.

C.5. Simplified parameter mapping

In the simplified mapping, we start from the relation (C.22) between the unbound diffusion coefficient D_{ub} and the basic time scale τ for the unbound motion. This time scale is now used for the bound movements as well. The unbinding probability ε_o is then chosen via

$$\varepsilon_o \equiv \frac{1}{1 + \Delta t_b/\tau} \tag{C.23}$$

and the bound state velocity v_b determines the hopping probabilities α and $\beta = \zeta\alpha$ via

$$\alpha - \beta = \alpha(1-\zeta) = (1-\varepsilon_o)\frac{\tau v_b}{\ell}\ , \tag{C.24}$$

where the normalization condition $\alpha + \beta + \gamma + \varepsilon_o = 1$ has been used.

Compared to the more elaborate parameter mapping with two time scales τ and τ_b, the simplified mapping leads to a larger value of γ which is typically close to 1. In addition, the simplified mapping does not incorporate the precise value for the bound diffusion coefficient D_b and the randomness parameter $\pi_r = 2D_b/\ell v_b$ as defined by (C.6).

References

[1] B. Alberts, D. Bray, A. Johnson, J. Lewis, M. Raff, K. Roberts, P. Walter, Essential Cell Biology: An Introduction to the Molecular Biology of the Cell, Garland, New York, 1998.
[2] J. Howard, Mechanics of Motor Proteins and the Cytoskeleton, 1 ed., Sinauer, New York, 2001.
[3] M. Schliwa, G. Woehlke, Molecular Motors, Nature 422 (2003) 759–765.
[4] K. Svoboda, C.F. Schmidt, B.J. Schnapp, S.M. Block, Direct observation of kinesin stepping by optical trapping interferometry, Nature 365 (1993) 721–727.
[5] M. Rief, R.S. Rock, A.D. Mehta, M.S. Mooseker, R.E. Cheney, J.A. Spudich, Myosin V stepping kinetics: a molecular model for processivity, Proc. Nat. Acad. Sci. USA 97 (2000) 9482–9486.
[6] G. Cappello, M. Badoual, A. Ott, J. Prost, Kinesin motion in the absence of external forces characterized by interference total internal reflection microscopy, Phys. Rev. E 68 (2003) 021907.
[7] L. Wang, C.-I. Ho, D. Sun, R.K.H. Liem, A. Brown, Rapid movement of axonal neurofilaments interrupted by prolonged pauses, Nat. Cell Biol. 2 (2000) 137–141.
[8] J.V. Shah, D.W. Cleveland, Slow axonal transport: fast motors in the slow lane, Curr. Opin. Cell Biol. 14 (2002) 58–62.
[9] D.D. Hurd, W.M. Saxton, Kinesin mutations cause motor neuron desease phenotypes by disrupting fast axonal transport in drosophila, Genetics 144 (1996) 1075–1085.

[10] M.A. Martin, S.J. Iyadurai, A. Gassman Jr., J.G. Gindhart, T.S. Hays, W.M. Saxton, Cytoplasmic dynein, the dynactin complex, and kinesin are interdependent and essential for fast axonal transport, Mol. Biol. Cell 10 (1999) 3717–3728.
[11] S. Konzack, Funtion des Kinesin Motorproteins KipA bei der Organisation des Mikrotubuli-Cytoskeletts und beim polaren Wachstum von Aspergillus nidulans, Doctoral thesis, University of Marburg, 2004.
[12] S. Konzack, P.E. Rischitor, C. Enke, R. Fischer, The role of the kinesin motor KipA in microtubule organization and polarized growth of Aspergillus nidulans, to be published.
[13] A. Einstein, Über die von der molekularkinetischen Theorie der Wärme geforderte Bewegung von in ruhenden Flüssigkeiten suspendierten Teilchen, Ann. Phys. 17/322 (1905) 549–560.
[14] M. von Smoluchowski, Zur kinetischen Theorie der Brownschen Molekularbewegung und der Suspensionen, Ann. Phys. 326 (1906) 756–780.
[15] R.D. Vale, D.R. Soll, I.R. Gibbons, One-dimensional diffusion of microtubules bound to flagellar dynein, Cell 59 (1989) 915–925.
[16] M. Guthold, X. Zhu, C. Rivetti, G. Yang, N.G. Thomson, S. Kasas, H.G. Hansma, B. Smith, P. Hansma, C. Bustamante, Direct observation on one-dimensional diffusion and transcription by *Escherichia coli* RNA polymerase, Biophys. J. 77 (1999) 2284–2294.
[17] A. Pais, 'Subtle is the Lord . . .'. The Science and the Life of Albert Einstein, Oxford University Press, Oxford, 1982.
[18] M.v. Smoluchowski, Gültigkeitsgrenzen des zweiten Hauptsatzes der Wärmetheorie, Phys. Zeitschr. 13 (1912) 88–121.
[19] H. Risken, The Fokker–Planck Equation: Methods of Solution and Applications, Springer, Berlin, 1989.
[20] H.S. Leff, A.F. Rex (Eds.), Maxwell's Demon: Entropy Information, Computing, Princeton U. P., Princeton, 1990.
[21] R.P. Feynman, R.B. Leighton, M. Sands, The Feynman Lectures on Physics Vol. I Mainly Mechanics, Radiation, and Heat, Addison-Wesley, Reading, MA, 1989.
[22] J. Monod, Zufall und Notwendigkeit. Philosophische Fragen der modernen Biologie, DTV, 1975.
[23] A. Yildiz, J.N. Forkey, S.A. McKinney, T. Ha, Y.E. Goldmann, P.R. Selvin, Myosin V walks hand-over-hand: single fluorophore imaging with 1.5-nm localization, Science 300 (2003) 2061–2065.
[24] C.L. Asbury, A.N. Fehr, S.M. Block, Kinesin moves by an asymmetric hand-over-hand mechanism, Science 302 (2003) 2130–2134.
[25] W.R. Schief, R.H. Clark, A.H. Crevenna, J. Howard, Inhibition of kinesin motility by ADP and phosphate supports a hand-over-hand mechanism, Proc. Natl. Acad. Sci. USA 101 (2004) 1183–1188.
[26] A. Yildiz, M. Tomishige, R.D. Vale, P.R. Selvin, Kinesin walks hand-over-hand, Science 303 (2004) 676–678.
[27] W. Hua, J. Chung, J. Gelles, Distinguishing inchworm and hand-over-hand processive kinesin movement by neck rotation measurements, Science 295 (2002) 844–848.
[28] R. Lipowsky, T. Harms, Molecular motors and nonuniform ratchets, Eur. Biophys. J. 29 (2000) 542–548.
[29] R. Lipowsky, Molecular motors and stochastic models, in: J. A. Freund, T. Pöschel (Eds.), Stochastic Processes in Physics Chemistry and Biology, Lecture Notes in Physics, vol. 557, Springer, Heidelberg, 2000, pp. 21–31.
[30] R. Lipowsky, Universal aspects of the chemo-mechanical coupling for molecular motors, Phys. Rev. Lett. 85 (2000) 4401–4404.
[31] R. Lipowsky, N. Jaster, Molecular motor cycles: from ratchets to networks, J. Stat. Phys. 110 (2003) 1141–1167.
[32] N. Jaster, Ratchet models of molecular motors, Doctoral Thesis, University of Potsdam, 2003.
[33] J. Prost, J.-F. Chauwin, L. Peliti, A. Ajdari, Asymmetric pumping of particles, Phys. Rev. Lett. 72 (1994) 2652–2655.
[34] F. Jülicher, A. Ajdari, J. Prost, Modeling molecular motors, Rev. Mod. Phys. 69 (1997) 1269–1281.
[35] A. Kolomeisky, B. Widom, A simplified "ratchet" model of molecular motors, J. Stat. Phys. 93 (1998) 633–645.

[36] M.E. Fisher, A. Kolomeisky, Simple mechanochemistry describes the dynamics of kinesin molecules, Proc. Natl. Acad. Sci. USA 98 (2001) 7748–7753.
[37] P. Reimann, Brownian motors: noisy transport far from equilibrium, Phys. Rep. 361 (2002) 57–265.
[38] K. Visscher, M.J. Schnitzer, S.M. Block, Single kinesin molecules studied with a molecular force clamp, Nature 400 (1999) 184–189.
[39] K.J. Böhm, R. Stracke, P. Mühling, E. Unger, Motor protein-driven unidirectional transport of micrometer-sized cargoes across isopolar microtubule arrays, Nanotechnology 12 (2001) 238–244.
[40] R. Lipowsky, S. Klumpp, T.M. Nieuwenhuizen, Random walks of cytoskeletal motors in open and closed compartments, Phys. Rev. Lett. 87 (2001) 108101/1-108101/4.
[41] T.M. Nieuwenhuizen, S. Klumpp, R. Lipowsky, Walks of molecular motors in two and three dimensions, Europhys. Lett. 58 (2002) 468–474.
[42] S. Klumpp, R. Lipowsky, Traffic of molecular motors through open tube-like compartments, J. Stat. Phys. 113 (2003) 233–268.
[43] T.M. Nieuwenhuizen, S. Klumpp, R. Lipowsky, Random walks of molecular motors arising from diffusional encounters with immobilized filaments, Phys. Rev. E 69 (2004) 061911/1-061911/19.
[44] A. Ajdari, Transport by active filaments, Europhys. Lett. 31 (1995) 69–74.
[45] S. Klumpp, R. Lipowsky, Active diffusion driven by molecular motors, to be published.
[46] C.T. MacDonald, J.H. Gibbs, A.C. Pipkin, Kinetics of biopolymerization on nucleic acid templates, Biopolymers 6 (1968) 1–25.
[47] S. Katz, J.L. Lebowitz, H. Spohn, Nonequilibrium steady-states of stochastic lattice gas models of fast ionic conductors, J. Stat. Phys. 34 (1984) 497–537.
[48] J. Krug, Boundary-induced phase transitions in driven diffusive systems, Phys. Rev. Lett. 67 (1991) 1882–1885.
[49] M.R. Evans, D.P. Foster, C. Godreche, D. Mukamel, Spontaneous symmetry breaking in a one dimensional driven diffusive system, Phys. Rev. Lett. 74 (1995) 208–211.
[50] A.B. Kolomeisky, G.M. Schütz, E.B. Kolomeisky, J.P. Straley, Phase diagram of one-dimensional driven lattice gases with open boundaries, J. Phys. A: Math. Gen. 31 (1998) 6911–6919.
[51] R.K.P. Zia, L.B. Shaw, B. Schmittmann, R.J. Astalos, Contrasts between equilibrium and non-equilibrium steady states: computer aided discoveries in simple lattice gases, Computer Phys. Commun. 127 (2000) 23–31.
[52] T. Antal, G.M. Schütz, Asymmetric exclusion process with next-nearest-neighbor interaction: some comments on traffic flow and a nonequilibrium reentrance transition, Phys. Rev. E 62 (2000) 83–93.
[53] G.M. Schütz, Exactly solvable models for many-body systems far from equilibrium, in: C. Domb, J.L. Lebowitz (Eds.), Phase transitions and Critical Phenomena, vol. 19, Academic Press, London, 2001, pp. 3–251.
[54] A. Parmeggiani, T. Franosch, E.Frey, Phase coexistence in driven one-dimensional transport, Phys. Rev. Lett. 90 (2001) 086601/1-86601/4.
[55] V. Popkov, A. Rakos, R.D. Willmann, A.B. Kolomeisky, G.M. Schütz, Localization of shocks in driven diffusive systems without particle number conservation, Phys. Rev. E 67 (2003) 066117/1-066117/6.
[56] M.R. Evans, R. Juhasz, L. Santen, Shock formation in an exclusion process with creation and annihilation, Phys. Rev. E 68 (2003) 026117/1-066117/8.
[57] S. Klumpp, R. Lipowsky, Asymmetric simple exclusion processes with diffusive bottlenecks, Phys. Rev. E 70 (2004) 066104/1-066104/9.
[58] U. Henningsen, M. Schliwa, Reversal in the direction of movement of a molecular motor, Nature 389 (1997) 93–96.
[59] E.P. Sablin, R.B. Case, S.C. Dai, C.L. Hart, A. Ruby, R.D. Vale, R.J. Fletterick, Direction determination in the minus-end-directed kinesin motor ncd, Nature 395 (1998) 813–816.
[60] A. Lockhart, I.M.-T.C. Crevel, R.A. Cross, Kinesin and ncd bind through a single head to microtubules and compete for a shared MT binding site, J. Mol. Biol. 249 (1995) 763–771.
[61] S. Klumpp, R. Lipowsky, Phase transitions in systems with two species of molecular motors, Europhys. Lett. 66 (2004) 90–96.

[62] D.T. Woodrum, S.A. Rich, T.D. Pollard, Evidence for biased bidirectional polymerization of actin filaments using heavy meromyosin prepared by an improved method, J. Cell Biol. 67 (1975) 231–237.
[63] A. Orlova, E.H. Egelman, Cooperative rigor binding of myosin to actin is a function of F-actin structure, J. Mol. Biol. 265 (1997) 469–474.
[64] A. Vilfan, E. Frey, F. Schwabl, M. Thormählen, Y.-W. Song, E. Mandelkow, Dynamics and cooperativity of microtubule decoration by the motor protein kinesin, J. Mol. Biol. 312 (2001) 1011–1026.
[65] E. Muto, Is microtubule an active participant in the mechanism of motility?, Biophys. J. 80 (2001) 513a.
[66] S. Klumpp, T.M. Nieuwenhuizen, R. Lipowsky, Self-organized density patterns of molecular motors in arrays of cytoskeletal filaments, Biophys. J., submitted.
[67] T. Harms, R. Lipowsky, Driven ratchets with frozen disorder, Phys. Rev. Lett. 79 (1997) 2895–2898.
[68] T. Surrey, F. Nédélec, S. Leibler, E. Karsenti, Physical properties determining self-organization of motors and microtubules, Science 292 (2001) 1167–1171.
[69] D. Humphrey, C. Duggan, D. Saha, D. Smith, J. Käs, Active fluidization of polymer networks through molecular motors, Nature 416 (2002) 413–416.
[70] D. Pantaloni, C.L. Clainche, M.-F. Carlier, Mechanism of actin-based motility, Science 292 (2001) 1502–1506.
[71] S. Romero, C. Le Clainche, D. Didry, C. Egile, D. Pantaloni, M.F. Carlier, Formin is a processive motor that requires profilin to accelerate actin assembly and associated ATP hydrolysis, Cell 2004, submitted.
[72] D.K. Fygenson, J.F. Marko, A. Libchaber, Mechanics of microtubule-based membrane extension, Phys. Rev. Lett. 79 (1997) 4497–4500.
[73] M. Dogterom, M.E. Janson, C. Faivre-Moskalenko, A. van der Horst, J.W.J. Kerssemakers, C. Tanase, B.M. Mulder, Force generation by polymerizing microtubules, Appl. Phys. A 75 (2002) 331–336.
[74] N.G. van Kampen, Stochastic Processes in Physics and Chemistry, Elsevier, Amsterdam, 1992.
[75] G. Kirchhoff, Über die Auflösung der Gleichungen, auf welche man bei der Untersuchung der linearen Verteilung galvanischer Ströme geführt wird, Ann. Phys. Chem. 72 (1847) 497–508.
[76] J.A. Christiansen, The elucidation of reaction mechanisms by the method of intermediates in quasi-stationary concentrations, Adv. Catal. 5 (1953) 311–353.
[77] T.A. Bak, Contributions to the Theory of Chemical Kinetics, 1 ed., Benjamin, New York, 1963.
[78] T.L. Hill, Studies in irreversible thermodynamics, IV, Diagrammatic representation of steady state fluxes for unimolecular systems, J. Theoret. Biol. 10 (1966) 442–459.
[79] J. Schnakenberg, Network theory of microscopic and macroscopic behavior of master equation systems, Rev. Mod. Phys. 48 (1976) 571–585.
[80] W.T. Tutte, Graph Theory, Cambridge University Press, Cambridge, 2001.
[81] B. Bollobas, Modern Graph Theory, Springer, New York, 1998.
[82] W.D. Wallis, A Beginners Guide to Graph Theory, Birkhäuser, Basel, 2000.
[83] M.J. Schnitzer, S.M. Block, Kinesin hydrolyses one ATP per 8 nm step, Nature 388 (1997) 386–390.
[84] K. Luby-Phelps, Cytoarchitecture and physical properties of cytoplasm: volume, viscosity, diffusion, intracellular surface area, Int. Rev. Cytology—A Survey of Cell Biol. 192 (2000) 189–221.
[85] Y. Okada, N. Hirokawa, A processive single-headed motor: kinesin superfamily protein KIF1A, Science 283 (1999) 1152–1157.